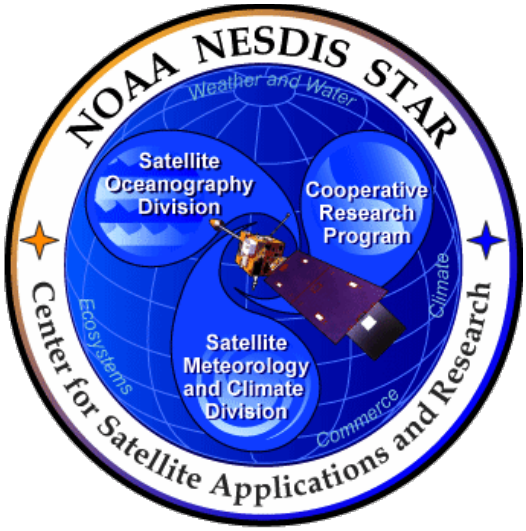

NOAA NESDIS
CENTER for SATELLITE APPLICATIONS and RESEARCH

ALGORITHM THEORETICAL BASIS DOCUMENT

Ice Thickness and Age from VIIRS, ABI, and METimage

Xuanji Wang, UW/CIMSS

Jeffrey R. Key, NOAA/NESDIS/STAR

Version 4.0

10 December 2019

TABLE OF CONTENTS

LIST OF FIGURES

LIST OF TABLES

LIST OF ACRONYMS

ABI - Advanced Baseline Imager
AIT - Algorithm Integration Team
APP-x – Extended AVHRR Polar Pathfinder
ATBD - algorithm theoretical basis document
AVHRR - Advanced Very High Resolution Radiometer
AWG - Algorithm Working Group
CIMSS - Cooperative Institute for Meteorological Satellite Studies
CIS - Canadian Ice Service
CSIM - CSM Sea Ice Model
CSM – Climate System Model
ECMWF - European Centre for Medium-Range Weather Forecasts
EPS-SG: EUMETSAT Polar System-Second Generation
F&PS - Function and Performance Specification
GCM – Global Circulation Model
GOCC - Generalized Orthogonal Curvilinear Coordinate
JPSS - Joint Polar Satellite System
MODIS - Moderate Resolution Imaging Spectroradiometer
MRD - Mission Requirements Document
MSG - Meteosat Second Generation
NASA - National Aeronautics and Space Administration
NCAR - National Center for Atmospheric Research
NCEP - National Centers for Environmental Prediction
NOAA - National Oceanic and Atmospheric Administration
NSIDC - National Snow and Ice Data Center
NWP - Numerical Weather Prediction
OTIM - One-dimensional Thermodynamic Ice Model
PIOMAS - Pan-Arctic Ice-Ocean Modeling and Assimilation System
POP - Parallel Ocean Program
RTM - Radiative Transfer Model
S-NPP - Suomi National Polar Orbiting Partnership
SCICEX - SCientific ICe EXpeditions
SEVIRI - Spinning Enhanced Visible and Infrared Imager
SHEBA - Surface HEat Balance of the Arctic Ocean
SIT – Sea Ice Temperature
SIC – Sea Ice Concentration
SSEC – Space Science and Engineering Center
TED - Thickness and Enthalpy Distribution
TOA – Top of Atmosphere
ULS – Upward Looking Sonar
UW – University of Wisconsin
VII: Visible Infrared Imager

ABSTRACT

This document provides a high level description of the physical basis for the determination of sea and lake ice thickness and age information, of each clear pixel data acquired by the Advanced Baseline Imager (ABI) on the GOES-R series of NOAA geostationary meteorological satellites, the Visible Infrared Imaging Radiometer Suite (VIIRS) on the Suomi National Polar Orbiting Partnership (S-NPP) satellite and the Joint Polar Satellite System (JPSS) series of NOAA polar-orbiting meteorological satellites, and the METimage (also called Visible Infrared Imager or VII) to be integrated in the EUMETSAT Polar System-Second Generation (EPS-SG) or Metop SG. Ice age is determined from the ice thickness information within the same algorithm module. Thus, the ice thickness and age are both described in this ATBD.

The core of the ice thickness and age algorithm is a One-dimensional Thermodynamic Ice Model (OTIM). Based on the surface energy budget, OTIM contains all components of the surface energy budget that are needed for the estimation of sea and lake ice thickness. Based on ice thickness, ice is classified into open water, new/fresh ice, grey ice, grey-white ice, thin first year ice, medium first year ice, thick first year ice, first year ice, and multi-year or older ice. Inevitably, OTIM contains parameterizations and/or assumptions of the sea and lake ice and associated snow characteristics of their physical properties, such as ice and snow conductivities, densities, and transmittances, if that kind of information is not available. The validation analysis indicates that the algorithm can meet the accuracy requirements of the Functional and Performance Specification (F&PS) as specified by NOAA GOES-R and JPSS programs.

1 INTRODUCTION

1.1 Purpose of This Document

The ice thickness and age algorithm theoretical basis document (ATBD) provides a high level description of the physical basis for the estimation of ice thickness and age for clear and cloudy pixels identified as ice covered with supplementary information from parameterization schemes and other products retrieved from the Advanced Baseline Imager (ABI) and Visible Infrared Imaging Radiometer Suite (VIIRS) flown on the GOES-R and JPSS series of NOAA geostationary and polar-orbital meteorological satellites, and also the METimage (also called Visible Infrared Imager or VII) to be integrated in the EUMETSAT Polar System-Second Generation (EPS-SG) or Metop SG. That supplementary information includes a cloud mask, snow depth, ice surface temperature, ice concentration, surface air temperature, surface air humidity, surface wind, and surface solar and thermal radiation fluxes. The ice thickness and age algorithm provides primary estimates of the ice thickness and age for each ABI or VIIRS or METimage pixel covered with ice. The ice thickness and age products are made available to all subsequent algorithms that require knowledge of ice information.

1.2 Who Should Use This Document

The intended users of this document are those interested in understanding the physical basis of the algorithm and how to use the output of this algorithm to estimate ice thickness and age for a particular application. This document also provides information useful to anyone maintaining or modifying the original algorithm.

1.3 Inside Each Section

This document is broken down into the following main sections.

- **System Overview**: Provides relevant details of the ABI and VIIRS and a brief description of the products generated by this algorithm.

- **Algorithm Description**: Provides all the detailed description of the algorithm including its physical basis, its input and its output.

- **Assumptions and Limitations**: Provides an overview of the current limitations of the approach and gives the plan for overcoming these limitations with further algorithm development.

1.4 Related Documents

This ATBD extends the related GOES-R and JPSS ATBD by adding information specific to METimage.

1.5 Revision History

Version 4.0 of this document was created by Xuanji Wang, Cooperative Institute for Meteorological Satellite Studies (CIMSS), University of Wisconsin-Madison, and Jeff Key, NOAA/NESDIS/STAR. It is intended to accompany the delivery of the version 4 algorithms to both the GOES-R AWG and the JPSS Algorithm Integration Teams (AIT), and the METimage on EPS-SG.

2 OBSERVING SYSTEM OVERVIEW

This section will describe the products generated by the ABI, VIIRS, and METimage Ice Thickness and Age algorithm and the requirements it places on the sensor and other products.

2.1 Products Generated

The ice thickness and age algorithm is responsible for the estimation of sea and lake ice thickness and age for all ABI, VIIRS or METimage pixels covered with ice. In terms of the ABI and JPSS MRDs, at the Threshold level, the ice-free areas are distinguished from first-year ice and older ice areas. The Goal requirement is to distinguish not only ice-free from first-year ice areas, but also to distinguish between the following types of ice: nilas, grey white, first-year thin, first-year medium, first-year thick, second-year, multiyear smooth and multiyear deformed ice. These categories are defined in terms of ice age. The ice thickness and age products will be used by other ABI, VIIRS or METimage algorithms that require knowledge of the ice information. The current ice thickness and age design has the ability to estimate sea and lake ice thickness up to 6 meters under both clear and cloudy conditions at night (no sunlight). It would also work during daytime, though the estimation might be more uncertain due to the complexities of ice and snow optical properties in the solar spectrum.

2.2 Instrument Characteristics

The ice thickness and age will be produced for each pixel observed by the ABI, VIIRS or METimage covered with ice. There are no direct ABI, VIIRS or METimage channels related to the algorithm which actually relies on some other retrieved products from ABI, VIIRS or METimage and parameterization schemes such as cloud mask and ice surface temperature that would use some or all ABI, VIIRS or METimage channels for their retrievals.

The algorithm relies on the accuracy of the other products and parameterization schemes such as the cloud mask, ice surface temperature, and radiation fluxes. The performance of the ice thickness and age algorithm is therefore sensitive to the accuracy of other ABI, VIIRS or METimage retrieved products. We will detail the required input parameters, the algorithm sensitivity to input uncertainties, and current validations in the following sections.

The ABI onboard the GOES-R has a wide range of applications in weather, oceanographic, climate, and environmental studies. ABI has 16 spectral bands (Table 1), with 2 visible bands, 5 near-infrared bands, and 9 infrared bands. The spatial resolution of ABI will be nominally 2 km for the infrared bands, 1 km for 0.47, 0.86, and 1.61 μm bands, and 0.5 km for the 0.64 μm visible band. ABI scans the full disk every 15 minutes, plus continental United States 3 times, plus a selectable 1000 km × 1000 km area every 30 s. ABI can also be programmed to scan the full disk every 5 minutes. Compared to previous GOES imagers, ABI offers more spectral bands and better spatial resolution. Especially, the newly added bands at 1.61 μm, and higher spatial

resolution at 0.64 μm allows for a better detection and monitoring of surface snow and ice (Schmit et al. 2005).

Table 1. Summary of the Current ABI Channel Numbers and Wavelengths.

Channel Number	***Wavelength (μm)***	***Direct Use in*** this algorithm
1	0.47	No
2	0.64	No
3	0.86	No
4	1.38	No
5	1.61	No
6	2.26	No
7	3.9	No
8	6.15	No
9	7.0	No
10	7.4	No
11	8.5	No
12	9.7	No
13	10.35	No
14	11.2	No
15	12.3	No
16	13.3	No

The VIIRS onboard the S-NPP and the JPSS satellites have 22 spectral bands covering wavelengths from 0.4 to 11.8 μm (Table 2). The S-NPP was launched on October 28, 2011; the first JPSS satellite, JPSS-1, was launched on November 18, 2017. Among the 22 bands, there are 5 high-resolution imagery bands (I-bands, 375 m spatial resolution at nadir), 16 moderate resolution bands (M-bands, 750 m spatial resolution at nadir), and one Day/Night Band (DNB, 750 m spatial resolution). The VIIRS swath width is 3000 km.

Table 2. Summary of the Current VIIRS Band Numbers and Spectral Ranges.

Band Number	***Wavelength (μm)***	***Direct Use in*** this algorithm
M1	0.402~0.422	No
M2	0.436~0.454	No
M3	0.478~0.498	No
M4	0.545~0.565	No
M5	0.662~0.682	No
M6	0.739~0.754	No
M7	0.846~0.885	No
M8	1.230~1.250	No
M9	1.371~1.386	No
M10	1.580~1.640	No
M11	2.225~2.275	No
M12	3.660~3.840	No
M13	3.973~4.128	No
M14	8.400~8.700	No
M15	10.263~11.263	No
M16	11.538~12.488	No

DNB	0.5~0.9	No
I1	0.600~0.680	No
I2	0.846~0.885	No
I3	1.580~1.640	No
I4	3.550~3.930	No
I5	10.500~12.400	No

METimage is an advanced multispectral imaging radiometer for meteorological applications. It is a follow-on to Advanced Very High Resolution Radiometer (AVHRR) on MetOp in the mid morning orbit. METimage will be integrated in the EPS-SG to be operational by 2022. The METimage has 20 spectral channels from 0.4 to 13.4 μm (Table 3), with several water vapor channels that VIIRS does not have. METimage swath width is about 2800 km, with a ground sampling distance of 500 m. Simulated METimage data, provided by EUMETSAT, are based on AVHRR product for clouds, Monitoring Atmospheric Composition and Climate (MACC) reanalysis for aerosols, ECMWF reanalysis for atmospheric state, and MOIDS albedo climatology, and simulated by the radiative transfer model of ARTDECO (Laboratoire d'Optique Atmosphérique at the Université de Lille-1).

Table 3. Summary of the METimage (VII) channel numbers and wavelengths.

Channel Number	***Wavelength (μm)***	***Bandwidth ((μm)***
VII-4	0.443	0.03
VII-8	0.555	0.02
VII-12	0.670	0.02
VII-15	0.752	0.01
VII-16	0.763	0.01
VII-17	0.865	0.02
VII-20	0.914	0.02
VII-22	1.240	0.02
VII-23	1.375	0.04
VII-24	1.630	0.02
VII-25	2.250	0.05
VII-26	3.740	0.18
VII-28	3.959	0.06
VII-30	4.050	0.06
VII-33	6.735	0.37
VII-34	7.325	0.29
VII-35	8.540	0.29
VII-37	10.690	0.50

VII-39	12.020	0.50
VII-40	13.345	0.31

3 ALGORITHM DESCRIPTION

Complete description of the algorithm at the current level of maturity (which will improve with each revision).

3.1 Algorithm Overview

The ice thickness and age algorithm will use a One-dimensional Thermodynamic Ice Model (OTIM) developed by the investigators. OTIM is based on the surface energy balance and contains all components of the surface energy budget to estimate sea and lake ice thickness up to 6 meters. Ice age is based on ice thickness as follows:

- Free or Open water: thickness = 0
- New: $0.00 < \text{thickness} \leq 0.10$
- Grey: $0.10 < \text{thickness} \leq 0.15$
- Grey-white: $0.15 < \text{thickness} \leq 0.30$
- First year Thin: $0.30 < \text{thickness} \leq 0.70$
- First year Medium: $0.70 < \text{thickness} \leq 1.20$
- First year Thick: $1.20 < \text{thickness} < 1.80$
- First year: $0.00 < \text{thickness} < 1.80$
- Older: $\text{thickness} \geq 1.80$

Pros: Solid physical foundation with all components of surface energy budget considered. Capable of retrieving daytime and nighttime sea and lake ice thickness under both clear and cloudy sky conditions. Very computationally efficient compared to more complex models such as the Climate System Model (CSM) Sea Ice Model (CSIM). Its sole objective of retrieving ice thickness and age makes it easy to implement with the application of satellite products, flexible, fast and easy to maintain and improve later with more and accurate satellite derived products like radiative fluxes, ice surface temperature and snow depth over the ice.

Cons: The accuracy of input parameters, e.g., snow depth, surface air humidity, temperature, and wind, will impact the accuracy of ice thickness estimates. Daytime retrieval is sensitive to ice optical properties associated with ice type and thickness.

3.2 Processing Outline

The processing outline of this algorithm is summarized in the following chart. The algorithm is designed to run on segments of data. A segment is comprised of multiple scan lines.

High Level Flowchart of the Algorithm Illustrating the Main Processing Sections.

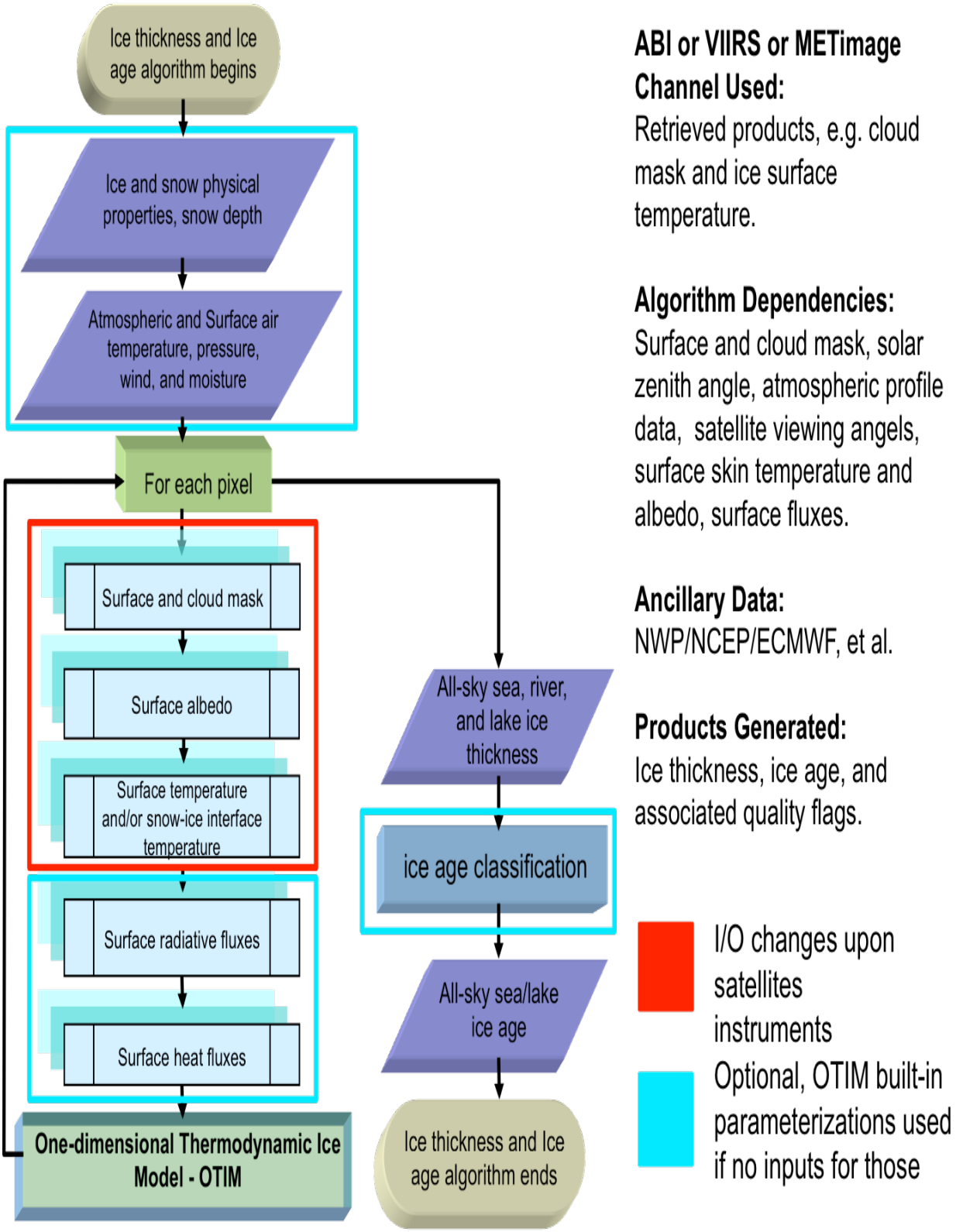

The Algorithm Dependency on Other ABI, VIIRS or METimage Products and Data Sources.

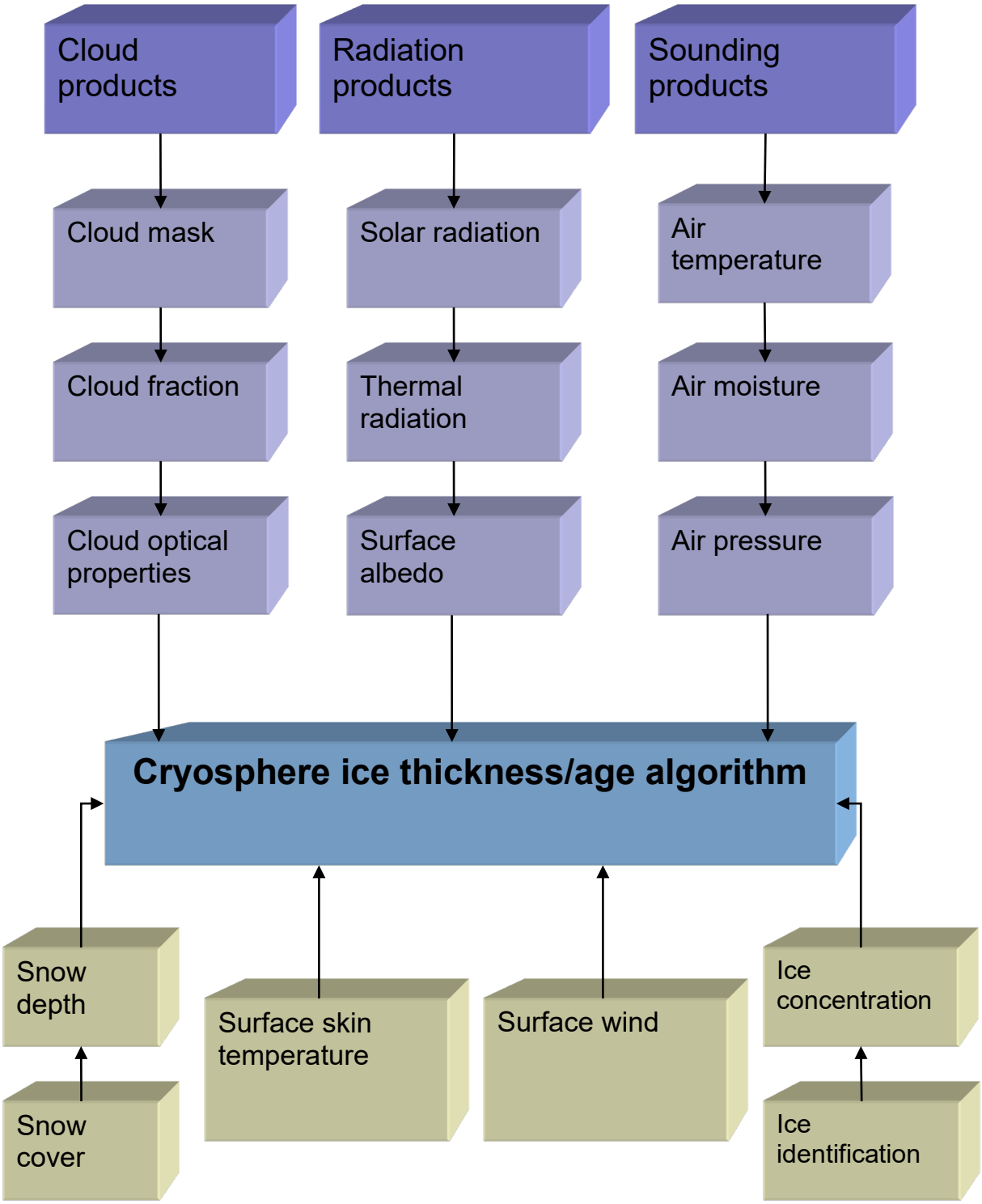

3.3 Algorithm Input

This section describes the inputs needed to process with this algorithm for ice thickness and age products. While this algorithm is derived for each pixel covered with ice, it does require knowledge of the surrounding atmosphere. In this version, the daytime retrieval was run and improved, though it might still be investigated in the next version due to the fact that complex solar radiation interactions might result in a larger uncertainty than with nighttime applications.

3.3.1 Primary Sensor Data

The list below contains the primary parameters data used by this algorithm, information that is derived mainly from the ABI, VIIRS or METimage observations and geolocation information.

- **Latitude**
- **Longitude**
- **Sensor viewing zenith angle**
- **Solar zenith angle**

3.3.2 Ancillary Data

The following lists and briefly describes the ancillary data required to run this algorithm, information that is not included in the ABI, VIIIRS or METimage observations or geolocation data.

- **Land mask**
- **Ice and Snow Thermal Emissivity**
- **Ice and Snow Optical Properties (Albedo, Transmittance, Absorptivity)**
- **Ice and Snow Physical Properties (Density, Salinity, Conductivity, Contaminant)**
- **Surface Air Temperature**
- **Surface Humidity**
- **Surface Wind**

3.3.3 Derived Data

The following briefly describes the products from other ABI, VIIRS or METimage algorithms that this algorithm uses as input. These data are necessary in order to run the software that calculates ice thickness and sequentially ice age. These data are required information that is not included in the ABI, VIIRS or METimage observations or geo-location data.

- **Cloud mask & Cloud Fraction**
- **Ice surface skin temperature**
- **Ice mask and concentration**
- **Shadow Mask from Cloud height**

- **Sun glint flag from Cloud Mask**

3.4 Theoretical Description

Physical and statistical approaches are employed to estimate sea and lake ice thickness and age. In this document, a One-dimensional Thermodynamic Ice Model (OTIM) based on the surface energy budget, containing all components of the surface energy budget has been developed to estimate sea and lake ice thickness. Then based on the knowledge of ice thickness, ice is classified into open water, new/fresh ice, grey ice, grey-white ice, thin first year ice, medium first year ice, thick first year ice, first year ice, and multi-year or older ice. It inevitably involves parameterizations and/or assumptions of the sea and lake ice and associated snow characteristics, such as ice and snow conductivities, densities, and transmittances.

3.4.1 Physics of the Problem

The difficult task for any ice thickness and age estimation based on the thermodynamic theory is to exploit not only ice and snow micro-physical properties which are closely related to ice and snow types and contents but also its environmental conditions such as humidity, air temperature, wind, cloud cover, water salinity and current. In the testing stage of this algorithm, we have extensively used information from the extended AVHRR Polar Pathfinder (APP-x) product, which consists of AVHRR retrievals of surface and cloud properties with our retrieval tool CASPR (Key, 2002) for the period 1982-2016 over the Arctic, the NCAR/NCEP Reanalysis data, parameterization schemes for ice and snow micro-physical properties, and solar and thermal radiation flux parameterizations at the surface developed by other researchers. In addition this algorithm has been tested with the MODIS and SEVIRI data as well. While the current NCAR/NCEP Reanalysis fields often have errors in some critical fields, such as the surface air temperature and humidity over ice and snow, they provide needed and useful information. Nevertheless, parameterization schemes are often needed to estimate environmental conditions, especially for ice and snow areas.

The following sections describe the model details of the OTIM. This algorithm uses the OTIM to estimate sea and lake ice thickness. The OTIM treats day and night retrievals differently in terms of the residual heat flux estimation. When the sun is above the horizon, the solar radiation must be considered in the OTIM which makes the ice thickness estimation complicated due to the unknown ice and snow types resulting in inaccurate ice and snow optical property estimates in the solar spectrum. Nighttime retrievals of ice thickness are relatively easier and more accurate, with an analytical solution in the OTIM. The OTIM has been tested with AVHRR, MODIS, and SEVIRI data and validated with submarine and moored Upward Looking Sonar data, meteorological station measurements, and numerical model simulations.

3.4.2 One-dimensional Thermodynamic Ice Model (OTIM)

A slab model proposed by Maykut and Untersteiner (1971) is used here as a prototype model, the equation for energy conservation at the top surface (ice or snow) is

$$(1-\alpha_s)F_r - I_0 - F_l^{up} + F_l^{dn} + F_s + F_e + F_c = F_a$$

or

$$(1-\alpha_s)(1-i_0)F_r - F_l^{up} + F_l^{dn} + F_s + F_e + F_c = F_a \qquad (1)$$

where α_s is ice surface broadband albedo where ice may be covered with a layer of snow, F_r is downward solar radiation flux at the surface, I_0 is the solar radiation flux passing through the ice interior and i_0 is ice slab transmittance, F_l^{up} is upward longwave radiation flux from the surface, F_l^{dn} is downward longwave radiation flux from the atmosphere towards the surface, F_s is turbulent sensible heat flux at the surface, F_e is turbulent latent heat flux at the surface, F_c is conductive heat flux within the ice slab, F_a is residual heat flux that could be caused by ice melting and/or heat advection. By the definitions of the terms in the equation (1), α_s, F_r, I_0, F_l^{up}, F_l^{dn} should be always positive, and F_s, F_e, and F_c would be positive or negative in terms of the operational symbols used in the equation (1), and F_a is zero in the absence of a phase change. The details of each term will be addressed in the following subsections.

3.4.2.1 Solar Radiation at the Surface

The first term on the left-hand side of the equation (1), $(1-\alpha_s)\,F_r$, is net solar radiation flux at the surface. The surface broadband albedo over entire solar spectrum, α_s, can be input or estimated by Thomas C. Grenfell (1979) method. The other relatively simple approach to determine ice and snow surface albedo include model simulated constant values based on the ice and snow types as discussed by Tuomo M. Saloranta (2000), and the experimental and observational values for a variety of snow and ice surface conditions (Grenfell and Perovich, 2004) as shown in Figure 1 from Donald K. Perovich (1996).

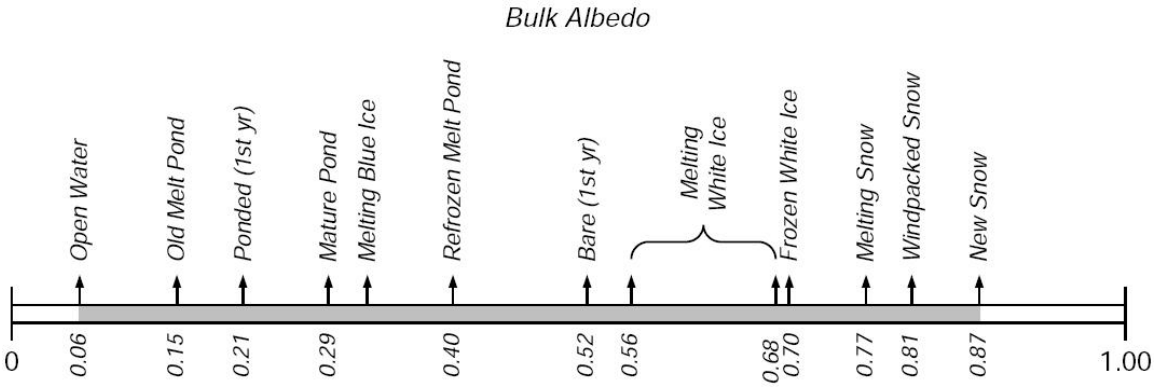

Figure 1. Range of observed values of total albedo for sea ice. The albedos are from Burt (1954), Chernigovskiy (1963), Langleben (1971), Grenfell and Maykut (1977), and Grenfell and Perovich (1984).

The downward shortwave radiation flux towards the surface, F_r, could also be input parameter for the OTIM or parameterized with model built-in parameterization schemes as described below. There are a number of parameterization schemes for the F_r estimation under both clear and cloudy sky conditions that are described in the following subsections. Key (1996) compared these schemes and discussed the use of which scheme would be better regarding the surface type, location, and atmospheric conditions.

3.4.2.1.1 Clear-sky Parameterizations of Solar Radiation

1. Shine and Henderson-Sellers (1985) scheme for the Arctic:

$$F_r^{clr} = 1368\mu^2[1.2\mu + (1.0 + \mu)\, e_a\, 10^{-3} + 0.046]^{-1} \qquad (2)$$

where μ = cosine of the solar zenith angle, $e_a = f \cdot e_{sa}$, e_a is surface water vapor pressure (hPa), e_{sa} is surface saturation water vapor pressure(hPa), f is relative humidity (%). So, knowing surface air temperature T_a (C) and relative humidity f, we can calculate e_a by

$$e_{sa} = 6.11*10.0\text{^}(7.5*T_a / (237.7 + T_a)) \qquad (3)$$

where $e_a = f\, e_{sa}$.

2. Moritz (1978) scheme for Baffin Bay, Canada:

$$F_r^{clr} = S_0\, \mu\, (0.47 + 0.47\, \mu) \qquad (4)$$

where S_0 is solar constant, μ is cosine of solar zenith angle.

3. Bennett (1982) scheme for the Arctic:

$$F_r^{clr} = 0.72\, S_0\, \mu \qquad (5)$$

where S_0 and μ are the same as the above. This one is recommended for its simplicity and acceptable accuracy.

3.4.2.1.2 Cloudy-sky Parameterizations of Solar Radiation

1. Berliand (1960) scheme:

$$F_r^{all} = F_r^{clr}\, (1 - x\, c - y\, c^2) \qquad (6)$$

where c is cloud fraction between 0~1. For land and ocean, $y=0.38$, $x=0.14$ at 85^o, 0.41 at 55^o, 0.38 at 45^o respectively; and $x=0.45$ and $y=0$ at 75^oN/S. Its performance is poor over oceans as tested.

2. Laevastu (1960) scheme for the mid-latitude ocean:

$$F_r^{all} = F_r^{clr} (1 - 0.6\, c^3) \quad (7)$$

3. Jacobs (1978) scheme for Baffin Island, Canada over the period June to October:

$$F_r^{all} = F_r^{clr} (1 - 0.33\, c) \quad (8)$$

4. Bennett (1982) scheme for Arctic sea ice:

$$F_r^{all} = F_r^{clr} (1 - 0.52\, c) \quad (9)$$

This one is recommended for its simplicity and acceptable accuracy for this study.

5. Shine (1984) scheme for high albedo surfaces such as ice and snow:

$$F_r^{cld} = (53.5 + 1274.5\, \mu)\, \mu^{0.5} / [1 + 0.139\, (1 - 0.9345\, \alpha_s)\, \tau] \quad (10)$$

$$F_r^{all} = [(1 - c)\, F_r^{clr} + c\, F_r^{cld}] \quad (11)$$

where α_s is surface broadband albedo (0~1), and τ is cloud optical depth.

3.4.2.2 Solar Radiation Passing through Ice Interior

The second term on the left-hand side of the equation (1), $I_0 = i_0\,(1-\alpha_s)F_r$, is the solar radiation flux passing through the ice interior. i_o is ice slab transmittance, i.e. the percentage of the net solar radiation flux that penetrates the ice, which can be input or estimated from parameterization schemes (e.g. Thomas G. Grenfell (1979))
In the first approximation, the parameter i_o for the percentage of penetrating shortwave radiation into snow is kept zero, and i_o for ice is calculated linearly as a function of cloudiness as given in Grenfell and Maykut's 1977 paper listed below:

$i_o = 0.18(1-c) + 0.35c$ for white ice thickness less than 0.1 m,

$i_o = 0.43\,(1-c) + 0.63c$ for blue ice thickness less than 0.1 m,

where c is cloud fraction.

3.4.2.3 Upward Longwave Radiation from the Surface

The third term on the left-hand side of the equation (1), F_l^{up}, is upward longwave radiation flux from surface that can be easily estimated with following formulae:

$$F_l^{up} = \varepsilon \sigma T_s^4 \quad (12)$$

where ε is longwave emissivity of the ice or snow surface, $\sigma = 5.6696*10^{-8}\ W\ m^{-2}\ deg^{-4}$ is the Stefan-Boltzman constant, and T_s is surface skin temperature in K. For simplicity, here ice emissivity of *0.988* is used. Even though some pixels contain a small portion of open water or snow surface, the error in emissivity from improperly defining the surface type is small because snow emissivity at 0^o look angle is *0.995*, very close to the value of *0.987* for ice and *0.988* for water (Rees, 1993). Due to the substance heterogeneity, both reflectance and emissivity are geometrically considered, e.g. bidirectional reflecting property of a plant.

3.4.2.4 Downward Longwave Radiation towards the Surface

The fourth term on the left-hand side of the equation (1), F_l^{dn}, is downward longwave radiation flux from the atmosphere towards the surface that can be parameterized by following schemes.

3.4.2.4.1 Clear-sky Parameterizations of Longwave Radiation

1. Yu and Rothrock (1996) scheme:

$$F_l^{dn} = \varepsilon^* \sigma T_a^4 \quad (13)$$

where $\varepsilon^* = 0.7855\ (1 + 0.2232\ c^{2.75})$ is an effective emissivity for the atmosphere and T_a is the near-surface air temperature at *2* m above the surface, and c is fractional cloud cover.

2. Efimova (1961) scheme:

$$F_{l,clr}^{dn} = \sigma T_a^4\ (0.746 + 0.0066\ e_a) \quad (14)$$

where e_a is water vapor pressure (*hPa*).

3. Ohmura (1981) scheme for the temperature range *243-289K*:

$$F_{l,clr}^{dn} = \sigma T_a^4\ (8.733*10^{-3}\ T_a^{0.788}) \quad (15)$$

where σ, T_a are the same as above. This one is recommended for the simplicity and acceptable accuracy in this work.

4. Maykut and Church (1973) scheme for the temperature range of *244-277K*:

$$F_{l,clr}^{dn} = 0.7855\ \sigma T_a^4 \quad (16)$$

where σ, T_a are the same as above.

5. Andreas and Ackley (1982) scheme for the Arctic and Antarctica regions:

$$F_{l,clr}^{dn} = \sigma T_a^4 (0.601 + 5.95*10^{-5} e_a^{1500/Ta}) \quad (17)$$

where σ, T_a are the same as above, e_a is the near-surface water vapor pressure (hPa).

3.4.2.4.2 Cloudy-sky Parameterizations of Longwave Radiation

1. Yu and Rothrock (1996) scheme:

$$F_l^{dn} = \varepsilon^* \sigma T_a^4 \quad (18)$$

where $\varepsilon^* = 0.7855 (1 + 0.2232 c^{2.75})$ is an effective emissivity for the atmosphere and T_a is the near-surface air temperature at 2 m above the surface, and c is fractional cloud cover.

2. Jacobs (1978) scheme for Arctic summer and winter:

$$F_l^{dn} = F_{l,clr}^{dn} (1 + 0.26\, c) \quad (19)$$

where c is fractional cloud cover. This one is recommended for the simplicity and acceptable accuracy in this work.

3. Maykut and Church (1973) scheme over *244-277K*:

$$F_l^{dn} = F_{l,clr}^{dn} (1 + 0.22\, c^{2.75}) \quad (20)$$

where c is fractional cloud cover.

4. Zillman (1972) scheme:

$$F_l^{dn} = F_{l,clr}^{dn} + \sigma T_a^4\, 0.96 (1 - 9.2*10^{-6} T_a^2) c \quad (21)$$

5. Schmetz et al (1986) scheme:

$$F_l^{dn} = F_{l,clr}^{dn} + (1 - \varepsilon_0)\, C\, \varepsilon_c\, \sigma T_0^4 \exp[(T_B + T_0) / 46] \quad (22)$$

where ε_0 is the effective sky emittance, ε_c is cloud emissivity, T_0 is the near-surface air temperature, and T_B is cloud base temperature.

3.4.2.5 Turbulent Sensible Heat Flux

The fifth term on the left-hand side of the equation (1), F_s, is the turbulent sensible heat flux at the surface that can be calculated by following formulae if it is an unknown variable in the OTIM.

$$F_s = \rho_a c_p C_s u (T_a - T_s) \quad (23)$$

where ρ_a is the air density (standard value of *1.275* kg·m^{-3} at 0°C and 1000 hPa), c_p is the specific heat of wet air that should be calculated from Eq. (25.1) with wet air specific humidity q, C_s is the bulk transfer coefficients for turbulent sensible heat flux between air and ice surface (Yu chose C_s = *0.003* for very thin ice, and *0.00175* for thick ice, *0.0023* for neutral stratification as suggested by Lindsay (1998) in his energy balance model for thick arctic pack ice), u is surface wind speed, T_a is near surface air temperature at *2* m above the surface, and T_s is surface skin temperature.

$$C_p = C_{pd}(1 - q + \frac{C_{pv}}{C_{pd}} q) \quad (23.1)$$

where C_{pv} is the specific heat of water vapor at constant pressure (1952 J K^{-1} kg^{-1}), and C_{pd} is the specific heat of dry air at constant pressure (1004.5 J K^{-1} kg^{-1}), so C_p can simply be written as C_p=1004.5·(1+0.9433·q).

The wet air density ρ_a can be calculated using gas law with given surface air pressure P_a (hPa), surface air virtual temperature T_v (K), and gas constant R_{gas} (287.1 J kg^{-1} K^{-1}) by Eq. 25.2.

$$\rho_a = \frac{100 P_a}{R_{gas} T_v} \quad (23.2)$$

where T_v=(1 + 0.608·q)·T_a, q is wet air specific humidity (kg/kg).

3.4.2.6 Turbulent Latent Heat Flux

The sixth term on the left-hand side of the equation (1), F_e, is turbulent latent heat flux at the surface that can be calculated by following formulae if it is an unknown variable in the OTIM.

$$F_e = \rho_a L C_e u (w_a - w_{sa}) \quad (24)$$

where ρ_a is air density, L is latent heat of vaporization (*2.5*·10^6 J·kg^{-1}) which should includes the latent heat fusion/melting (*3.34*·10^5 J·kg^{-1}) if the surface is below freezing, C_e is the bulk transfer coefficients for latent heat flux of evaporation, u is surface wind speed, w_a is the air mixing ratio at 2 m, w_{sa} is the mixing ratio at the surface. Mixing ratio is very close to specific humidity in magnitude, $w = q/(1-q) \cong q$, where q is the specific humidity.

The bulk transfer coefficients C_e for latent heat flux is a function of wind speed and air-sea ice temperature difference which can be parameterized as described by Bentamy et al (2003),

$$C_e = \{ a \exp[b (u + c)] + d/u + 1 \} x10^{-3}, \quad (24.1)$$

where a=-0.146785, b=-0.292400, c=-2.206648, and d=1.6112292. The C_e values range between 0.0015 and 0.0011 for wind speeds between 2 and 20 m s^{-1}. Schroder et al's study (2003) indicated that C_e values are always around $1.0x10^{-3}$ except for rough multi-year ice which has C_e value of $1.3x10^{-3}$, and C_s value of $1.5x10^{-3}$ from six ice categories that are gray young ice, mixture of gray and white ice and leads, rough multi-year ice, step change between ice and water, loose ice fields, and grease ice (Table 2 in their paper). Another parameterization scheme of C_e was developed by Kara et al (2000) for use in general circulation model. They related C_e to both surface wind speed and air-sea temperature difference, the fitted expression are as follows:

$$C_e = C_{e0} + C_{e1}\,(T_s - T_a) \qquad (24.2)$$

$$C_{e0} = [0.994 + 0.061\cdot\hat{u} - 0.001\cdot\hat{u}^2]\cdot 10^{-3} \qquad (24.3)$$

$$C_{e1} = [-0.020 + 0.691\cdot(1/\hat{u}) - 0.871\cdot(1/\hat{u})^2]\cdot 10^{-3} \qquad (24.4)$$

where the wind speed is limited to the interval $\hat{u}$ = max[3.0, min(27.5, u)] to suppress the underestimation of the quadratic fit when u > 27.5 m s^{-1}.

Because the C_s values are so close in value to the C_e for sea water, a linear relationship between C_e and C_s rather than determine independent C_{s0} and C_{s1} coefficients. This also helps to reduce the cost of computing the sensible heat flux in GCMs, the simplest representative linear formulation is found to be $C_s=0.96\cdot C_e$ with a negligible intercept ($3.6\cdot 10^{-6}$) as reported by Kara et al. (2000), we use $C_s=0.98\cdot C_e$ in our model for air-sea ice interface turbulent heat transfer.

3.4.2.7 Conductive Heat Flux

The seventh term on the left-hand side of the equation (1), F_c, is conductive heat flux within the ice slab. It is neither input nor calculated in the current algorithm. The Ice thickness retrievals are done based on the analytical solution for the case with unknown Conductive Flux. Conductive Heat Flux defined by Yu and Rathorck (1996) is as follows.

$$F_c = \gamma\,(T_f - T_s) \qquad (25)$$

where $\gamma = (k_i\,k_s) / (k_s\,h_i + k_i\,h_s)$, T_f is water freezing temperature and can be derived from a simplified relationship of $T_f = -0.055\cdot S_w$, where S_w is the salinity of seawater and assumed to be ***31.0*** parts per thousand (ppt) for the Beaufort Sea and ***32.5*** ppt for the Greenland Sea, which means T_f is in the unit of degree Celsius. h_s is snow depth, and h_i is ice thickness. k_s is the conductivity of snow which can be formulated by $k_s=2.845\cdot 10^{-6}\rho_{snow}^2 + 2.7\cdot 10^{-4}\cdot 2.0^{(Tsnow-233)/5}$ (Ebert and Curry, 1993), ρ_{snow} is snow density ranging from ***225*** kg·m^{-3} (new snow) ~ ***450*** kg·m^{-3} (water-soaked snow), T_{snow} is snow temperature in Kelvin. The k_s can be further simplified as $k_s=2.22362\cdot 10^{-5.655}(\rho_{snow})^{1.885}$ (Yen, Y.-C., 1981). Usually, the k_s is assumed ***0.31*** in some applications. The k_i is the conductivity of ice that can be estimated by $k_i = k_0 + \beta\cdot S_i/(T_i - 273)$ (Untersteiner's, 1964), where $\beta=0.13$ W·m^{-2}·kg^{-1}, $k_0=2.22\cdot(1-0.00159\cdot T_i)$ W·m^{-1}·K^{-1} is the conductivity of pure ice (Curry and Webster, 1999). S_i is sea ice salinity, T_i is the temperature within the ice slab. Some experimental relative relationships between h_s and h_i, T_i and T_s, S_i and h_i exist as described in the following subsections. See Appendix A for the derivation of the Equation 25 for a two-layer system with snow over ice.

3.4.2.8 Solving the OTIM for Ice Thickness

3.4.2.8.1 Relationship between Snow Depth and Ice Thickness

Doronin (1971) used the following relationship to estimate snow depth in terms of ice thickness, which was also used in Yu's paper (1996):

$h_s = 0$, for $h_i < 5$ cm;
$h_s = 0.05 \cdot h_i$, for 5 cm $\leq h_i \leq$ 20 cm;
$h_s = 0.1 \cdot h_i$, for $h_i >$ 20 cm.

In reality, snow accumulation over the ice may not obey the relationship above, and most likely not be that simple. So we set snow depth as one input variable in the OTIM once climate data or measurements are available. In case there are no snow depth data available, snow depth estimate could be given in terms of date and hemisphere from snow climatological data.

3.4.2.8.2 Relationship between Surface Temperature and Ice Temperature

The ice temperature T_i is one important factor affecting ice conductivity calculation, which may be significantly different from the surface skin temperature that would be measured or retrieved with remote sensing data. In general, we can obtain surface skin temperature T_s through satellite retrieval techniques more or less directly, but not T_i if the surface is covered with thick snow. Yu and Rothrock (1996) suggested that assuming T_i equal to T_s can cause 5% and 1% errors when ice is 5 cm thick and 100 cm thick, respectively. That assumption may be valid when it is dark because when it is daytime most of solar radiation is reflected back to the atmosphere from the snow layer; very little of the solar radiation can actually reach the interface of the ice and snow, especially for new snow. Thus the surface skin temperature T_s is the surface snow temperature, which may differ from the ice temperature significantly. This can result in a large uncertainty in the ice conductivity calculation, resulting in a large error in the calculated ice thickness. This is one of major error sources for the daytime retrieval of ice thickness with the OTIM. More work should be done to correct the solar radiation treatment in the OTIM for sunlit conditions.

3.4.2.8.3 Relationship between Sea Ice Thickness and Sea Ice Salinity

There are some experimental relationships between sea ice thickness h_i and sea ice salinity S_i as listed below.

1. Cox and Weeks (1974) scheme:

$S_i = 14.24 - 19.39 \cdot h_i$, for $h_i \leq$ 0.4 m,
$S_i = 7.88 - 1.59 \cdot h_i$, for $h_i >$ 0.4 m.

2. Jin, Stamnes, and Weeks (1994) scheme:

$S_i = 17.0 - 31.63 \cdot h_i$, for $h_i \le 0.3$ m,
$S_i = 8.0 - 1.63 \cdot h_i$, for $h_i > 0.3$ m.

3. Kovacs (1996) scheme:

$S_i = 4.606 + 0.91603/h_i$, for 0.10 m $\le h_i \le$ 2.0 m.

We modify above schemes from Jin et al (1994) and Kovacs (1996) in the OTIM for the ice thickness greater than 2.0m as listed below:

$S_i = 2.619 + 1.472/h_i$, for 0.10 m $\le h_i \le$ 6.0 m.

3.4.2.8.4 Analytical Solution

The OTIM can be solved for ice thickness analytically in terms of input options and variable status as described in the following subsections. First let's rewrite the Eq. (1) into the following form

$$\boldsymbol{F_C + F = 0} \qquad \textit{(26)}$$

where the Net Flux, $F = -F_l^{up} + F_l^{dn} + F_s + F_e - F_A$, and $F_A = F_a - (1-\alpha)(1-i_o)F_r$ The residual heat flux F_A now includes ice slab absorbed solar radiation flux. In certain circumstances, no retrieval will be done to avoid possible cloud contaminated and/or melting pond pixels that will cause unrealistic ice thickness estimate. The net flux F and ice surface temperature T_s is used to evaluate whether or not retrieval will be done in terms of their values from our experience. The retrieval will not be done when 1) -28<F<8.0 and T_s > 268 for daytime clear sky condition, 2) -5<F<5.0 and T_s > 268 for daytime cloudy sky condition, 3) -18<F<8.0 and T_s > 258 for nighttime clear sky condition, and 4) -5<F<5.0 and T_s > 258 for nighttime cloudy sky condition.

Let $T_f - T_s = T_r$ and from Eq. (26) we have

$$F_C = \Upsilon \left(T_f - T_s\right) = \frac{k_i \; k_s}{k_s \; h_i + k_i \; h_s}(T_r) \qquad \textit{(27)}$$

T_f is water freezing temperature and can be derived from a simplified relationship

$T_f = -0.055 * S_w$ where S_w is the salinity of seawater

S_w is assumed to be 31.0 $parts \;\; per \;\; thousand \;\; (ppt)$ for the Beaufort Sea and 32.5 ppt for the Greenland Sea, which means T_f is in the unit of degree Celsius. h_s is snow depth, and h_i is ice thickness. k_s is the conductivity of snow which can be formulated as

$k_s=2.845\cdot10^{-6}\rho_{snow}^2+2.7\cdot10^{-4}\cdot2.0^{(Tsnow-233)/5}$ (Ebert and Curry, 1993), ρ_{snow} is snow density ranges from ***225*** kg·m^{-3} (new snow) ~ ***450*** kg·m^{-3} (water-soaked snow), T_{snow} is snow temperature in Kelvin. k_s can be further simplified as

$k_s=2.22362\cdot10^{-5.655}(\rho_{snow})^{1.885}$ (Yen, Y.-C., 1981)

Usually, k_s is assumed ***0.31*** in some applications. The k_i is the conductivity of ice that can be estimated using

$k_i=k_0+\beta\cdot S_i/(T_i-273)$ (Untersteiner's, 1964), where $\beta=0.13$ W·m^{-2}·kg^{-1} and $k_0=2.22\cdot(1-0.00159\cdot T_i)$ W·m^{-1}·K^{-1} is the conductivity of pure ice (Curry and Webster, 1999).

S_i is sea ice salinity, T_i is the temperature within the ice slab. Some experimental relative relationships between h_s and h_i, T_i and T_s, S_i and h_i exist as described in the following sections.

$$F_C = \Upsilon\ (T_f - T_s) = \frac{k_i\ k_s}{k_s\ h_i + k_i\ h_s}\ T_r$$

We have $S_i = S_o + \frac{S_1}{\mathrm{h}}, \quad where\ \ S_o = 2.619,\ \ S_1 = 1.472,\ \ and\ \ T_o = 273.15$

Let $T_i - T_o = T_k \quad and\ \ k_oT_k + \beta S_o = g$

$$k_i = \frac{(k_oT_k + \beta S_o)h + \beta S_1}{T_k\ \ h} = \frac{gh + \beta s_1}{T_k h}$$

We have,

$$\Upsilon = \frac{k_iK_s}{k_sh_i + k_ih_s} = \frac{k_s[(k_0T_k + \beta S_o)h + \beta S_1]}{k_sT_k\ \ h^2 + gh_sh + \beta S_1h_s} = \frac{k_s(gh + \beta S_1)}{k_sT_k\ \ h^2 + gh_sh + \beta S_1h_s}$$

Therefore,

$$F_C = \frac{k_sT_r(gh + k_2)}{k_sT_kh^2 + g_2h + k_2h_s}, \qquad where\ \ k_2 = \beta s_1$$

Therefore, $$F_C = \frac{k_sT_r(gh + \beta s_1)}{k_sT_kh^2 + g_2h + k_2h_s} \qquad (\mathbf{28})$$

Based on Eq. (26), we have $F_C + F = 0$

Therefore, $$\frac{k_s T_r(gh + \beta s_1)}{k_s T_k h^2 + g_2 h + k_2 h_s} + F = 0$$

We can rewrite

$$Fk_s T_k h^2 + (k_s T_r g + F g_2)h + (k_s T_r + F h_s)k_2 = 0 \qquad (\mathbf{29})$$

$$Let \quad a = Fk_s T_k, \qquad b = k_s T_r g, \qquad c = (k_s T_r + F h_s)k_2$$

Then we rewrite Eq (30) in the form $ah^2 + bh + c = 0$

The solution for the monadic quadratic equation is

$$h = \frac{-b \pm \sqrt{b^2 - 4ac}}{2a}$$

$when \quad b^2 - 4ac > 0.0$ there are real solutions as follows

$$h = \frac{F g_2 + k_s T_r g}{k_s T_k F + k_2 h_s F + k_s k_2 k_2 T_r} \qquad (\mathbf{30})$$

3.4.2.8.5 Residual Heat Flux

The largest uncertainty in the above model for daytime retrieval is the unknown residual heat flux F_A not being zero in real world, which is large enough to be considered in the OTIM as an important term. Physically, F_A should be related to the surface and atmospheric conditions such as surface skin temperature, broadband albedo, air temperature, air humidity, surface wind speed, horizontal heat advection within ice and snow, and surface solar radiation if daytime. Here we set the F_A be a function of some surface and atmospheric variables including cosine and sine of ice melting and freezing days (cosmel, sinmel, cosfre, sinfre), snow depth (h_s), cosine of Solar zenith angle (cossol), surface downward longwave radiative flux (F_l^{dn}), and surface upward longwave radiative flux (F_l^{up}), surface downward solar radiative flux (F_r), surface sensible heat flux (F_s), and surface latent heat flux (F_e). A regression equation for the calculation of the residual heat flux was build up by using in-situ measurements of ice thickness from surface, submarine, buoy, mooring, and field campaigns data to calculate F_A first using this OTIM, and then stepwise regress technique was applied to build up a multi-regress equation for the F_A predictand calculation with above mentioned variables as predictors. There are four regression equations for estimating F_A in terms of four conditions that are daytime with/without profile data, and nighttime with/without profile data, respectively as listed below.

1) Daytime case with profile data

$$F_A = 54.65025 - 4.781119*cossol - 5.432518*cosfre + 4.144333*sinfre - 174.5416*h_s + 2.610399*F_r + 1.034201*F_l^{dn} - 1.107273*F_l^{up} + 0.9960775*F_s + 1.054412*F_e$$

2) Daytime case without profile data

$F_A = 20.82845 + 3.701520*sinmel - 6.441864*cosfre - 135.1727*h_s - 3.901515*F_r - 0.04905455*F_l^{dn} - 0.4591621*F_s - 1.368342*F_e$

3) Nighttime case with profile data

$F_A = 75.38058 + 13.53732*cossol - 58.50422*sinsol - 3.827107*cosmel + 9.249864*h_s + 1.052007*F_l^{dn} - 1.098335*F_l^{up} + 1.078749*F_s + 0.9728903*F_e$

4) Nighttime case without profile data

$F_A = 66.62647 - 13.80995*sinsol - 4.028092*cosmel + 0.9453123*F_l^{dn} - 1.108553*F_l^{up} + 1.118411*F_s$

Where cosmel = COS($2\pi \cdot J_m/366$), sinmel = SIN($2\pi \cdot J_m/366$), cosfre = COS($2\pi \cdot J_f/366$), and sinfre = SIN($2\pi \cdot J_f/366$). J_m and J_f are the Julian day numbers from the melting/freezing start dates, respectively. For example, if melting date is May 1, then $J_m = 10$ means the actual date is May 11.

3.4.2.8.6 Thermodynamic Process Adjustment

The One-dimensional Thermodynamic Ice Model (OTIM) is further improved by including a parameterization scheme for ice thermodynamic process of seasonal freeze-up and melt. To explicitly express ice thermodynamic process in the OTIM, a parameterization scheme was developed and implemented to further improve ice thickness retrieval. This is an addition to the residual heat flux adjustment from which the ice thermodynamic process is not considered. In the new parameterization, ice thickness is adjusted by a factor, called the thermodynamic factor $\boldsymbol{f_{td}}$, which is a function of the freeze-up and melt dates at a particular location. This improvement significantly improves the ice thickness retrieval, especially for the melt season, though it also affects the freeze-up season as well. The ice growing/melting will follow the modeled exponential curve, and the $\boldsymbol{f_{td}}$ can be estimated by an exponential function of location (latitude/longitude), melting/freezing start dates (month/day), current date (month/day), and modeled maximum/minimum melting/freezing rates at the location. The steps and equations to calculate the $\boldsymbol{f_{td}}$ are as below.

1) Get the changing rate at a location x by using two known rates and locations.

$R_x = (R_0*L_1 - R_1*L_0)/(L_1 - L_0) + ((R_1 - R_0)/(L_1 - L_0))*L_x$, Where L_1 and L_0 are the two latitudes where their changing rates are know as R_0 and R_1, therefore the changing rate R_x at the latitude L_x can be estimated. By default, latitudes L_0=50°N/S, L1=90°N/S, and the R_0=1.0 and R_1=2.0.

2) Get the $\boldsymbol{f_{td}}$ at a location by using exponential function

First to estimate normalized Julian day fraction number $D_x = (D_j - D_{m/f})/D_{period}$, where D_x is from 0~1 (normalized by period) based on the actual Julian day number D_j, and $D_{m/f}$ is the Julian day number when melting/freezing starts, and the D_{period} is the total number of days for melting/freezing period. By default, the melting/freezing date at a location L_x can be estimated by two known dates at two known locations just like the step 1.

Once we know D_x, then the thermodynamic factor $\boldsymbol{f_{td}}$ can be estimated in terms of melting/freeing period as below.

For the D_x in a freezing period

$Y = X^{**}(S*D_x)$, where X is exponential base X=10, and S is the shape control number S=1, therefore $\boldsymbol{f_{td}} = (Y-1.0)*(R_x - R_0)/(X^{**}S - 1) + R_0$.

For the D_x in a melting period

$Y = X^{**}(-1.0*S*D_x)$, where X is exponential base X=10, and S is the shape control number S=1, therefore $\boldsymbol{f_{td}} = (Y- X^{**}(-1.0*S))*(R_x - R_0)/(1.0 - X^{**}(-1.0*S)) + R_0$.

3.4.2.8.7 Physical dynamic Process Adjustment

To better estimate ice thickness, it is needed to consider ice physical dynamic process of ice motion such as ridging, rafting, and homocking processes, in addition to the energy balance at the interface. This is becoming extremely important when ice is moving towards the shore area and accumulated there to form thick ice due to the dynamic process. To explicitly express ice physical dynamic process in the OTIM, a parameterization scheme was developed and implemented in the OTIM to further improve ice thickness retrieval in addition to ice thermal dynamic process as OTIM is supposed to do. The OTIM estimated ice thickness was further adjusted by a factor, called physical-dynamic factor $\boldsymbol{f_{pd}}$, which is calculated from the parameterization scheme. This physical-dynamic factor $\boldsymbol{f_{pd}}$ finally is the function of a location, wind, and season. This improvement is now only applied to the ice thickness retrieval in the coastal areas along Canadian Archipelago where ice physical dynamic process plays a big role in ice thickness estimation.

Wind can play role in the ice thickness by physical dynamic process such as rafting and ridging. First, the wind adjustment factor f_{wind} is estimated by $f_{wind} = (30 - W)/30$, where W is wind speed. Second, the date adjustment factor f_{day} is calculated by $f_{day} = (f_0*d_1 - f_1*d_0)/(d_1 - d_0) + ((f_1 - f_0)/(d_0 - d_1))*d_x$, where d_o and d_1 are the two days with known adjustment factors f_0 and f_1. Third, the location adjustment factor f_{loc} is estimated by $f_{loc} = (f_0*L_1 - f_1*L_0)/(L_1 - L_0) + ((f_1 - f_0)/(L_0 - L_1))*L_x$, where L_o and L_1 are the two locations with known adjustment factors f_0 and f_1. Finally, the overall physical dynamic factor $\boldsymbol{f_{pd}}$ can be obtained by $\boldsymbol{f_{pd}} = f_{wind}*f_{day}*f_{loc}$.

3.4.2.9 Ice Age

The ABI and JPSS Mission Requirements Documents (MRD) require, at the Threshold level, that ice-free areas be distinguished from first-year ice and older ice areas. The Goal requirement is to distinguish not only ice-free from first-year ice areas, but also to distinguish between the following types of ice: nilas, grey white, first-year medium, first-year thick, second-year, multiyear smooth, and multiyear deformed, commonly called ice age. Generally speaking, older ice is thicker than younger ice. In essence, this assumption is valid as tested and verified by many other researchers (e.g., Tucker et al., 2001; Yu et al., 2004; Maslanik et al., 2007). So ice thickness is used as a proxy for ice age.

There is an internationally accepted terminology for ice form and conditions, coordinated by the WMO. This terminology is used by the Canadian Ice Service as the basis for reporting ice conditions, and adopted by this work, with minor modifications, for classifying ice into different categories. Refer to the *Manual of Standard Procedures for Observing and Reporting Ice Conditions* by the Canadian Ice Service, available at http://ice-glaces.ec.gc.ca/App/WsvPageDsp.cfm?Lang=eng&lnid=23&ScndLvl=no&ID=172.

Sea/Lake types

- **New**: A general term for recently formed ice which includes frazil ice, grease ice, slush and shuga. These types of ice are composed of ice crystals which are only weakly frozen together (if at all) and have a definite form only while they are afloat.
- **Nilas**: A thin elastic crust of ice, easily bending on waves and swell and under pressure growing in a pattern of interlocking "fingers" (finger rafting). Nilas has a matte surface and is ***up to 10 cm*** in thickness and may be subdivided into dark nilas and light nilas.
- **Grey Ice**: Young ice ***10-15 cm*** thick. Less elastic than nilas and breaks on swell. Usually rafts under pressure.
- **Grey-white Ice**: Young ice ***15-30 cm*** thick. Under pressure it is more likely to ridge than to raft.
- **Thin First-year Ice**: First-year ice of not more than one winter's growth, ***30-70 cm*** thick.
- **Medium First-year Ice**: First-year, ice ***70-120 cm*** thick.
- **Thick First-year Ice**: First-year ice ***120-180 cm*** thick.
- **Old Ice**: Sea ice which has survived at least one summer's melt. Topographic features generally are smoother than first-year ice, and ***more than 180 cm*** thick. May be subdivided into second-year ice and multi-year ice.
- **Second-year Ice**: Old ice which has survived only one summer's melt.
- **Multi-year Ice**: Old ice which has survived at least two summer's melt.

3.4.3 Algorithm Output

The final outputs of this algorithm are:

- Ice thickness
- Ice age
- Optional geophysical variables
- Quality control (QC) flags
- Product quality information (PQI)
- Metadata

These are described in Tables 4-8. The ice thickness values are in the range 0 ~ 6.0 m for both sea ice and lake ice. Ice age categories and descriptions of their meanings are given in Table 4.

Table 4. Output parameters and their definitions.

Definition	**Description**
Ice Thickness	Ice thickness is defined as the total vertical length of the ice under and above water surface. The reliable ice thickness retrieved from this algorithm ranges between ***0 ~ 6.0 m***.
Ice age 3 category	3 Category Ice Age
1: Open Water	Open water or free of ice with ice thickness being zero or less than ***0.1 cm***.
2: New Ice	First year ice (include grey ice, young ice, and first year ice) with ***0.1 cm - 180 cm*** in thickness
3: Old Ice	Older ice ***more than 180 cm*** thick. Smoother than first-year ice and include second year and multiyear ice
Ice age 8 category	8 Category Ice Age
1: Open Water	Open water or free of ice with ice thickness being zero or less than 0.1 cm.
2: New	Newly formed ice with a thin elastic crust, easily bending on waves and swell and under pressure growing in a pattern of interlocking “fingers” (finger rafting). Nilas has a matte surface and is ***up to 10 cm*** in thickness and may be subdivided into dark nilas and light nilas.
3: Grey	Young ice ***10-15 cm*** thick. Less elastic than nilas and breaks on swell. Usually rafts under pressure.
4: Grey-white	Young ice ***15-30 cm*** thick. Under pressure it is more likely to ridge than to raft.
5: First-year Thin	First-year ice of not more than one winter's growth, ***30-70 cm*** thick.
6: First-year Medium	First-year, ice ***70-120 cm*** thick.
7: First-year Thick	First-year ice ***120-180 cm*** thick.
8: Older Ice	Sea ice that has survived at least one summer's melt. Topographic features generally are smoother than first-year ice, and ***more than 180 cm*** thick. May be subdivided into second-year ice and multi-year ice. **First-year Ice:** Categories 2 ~ 7, ice thickness between 0.001 m and 1.80 m. **Second-year Ice**: Old ice which has survived only one summer's melt. **Multi-year Ice**: Old ice which has survived at least two summer's melt.

The algorithm can also output other optional parameters that are closely related to the surface energy budget and ice thickness retrieval. These optional outputs from OTIM are listed and described in Table 5. These optional output parameters will be implemented in the next version of the algorithm.

Table 5. Optional output parameters and their definitions.

Parameter	Unit	Description
Cloud mask	0 or 1	Clear or Cloudy over the ice surface, observed.
Surface broadband albedo	0 ~ 1	Ice/snow surface broadband albedo, modeled or in-situ measured, daytime only.
Ice Transmittance	0 ~ 1	Ice slab transmittance for solar radiation, modeled or measured, daytime only.
Surface incoming solar radiation flux	$W \cdot m^{-2}$	Incoming solar radiation flux at the surface, modeled or observed, daytime only.
Surface outgoing thermal radiation flux	$W \cdot m^{-2}$	Outgoing thermal radiation flux at the surface, modeled or observed.
Surface incoming thermal radiation flux	$W \cdot m^{-2}$	Incoming thermal radiation flux at the surface, modeled or observed.
Surface turbulent sensible heat flux	$W \cdot m^{-2}$	The turbulent sensible heat flux at the interface of ice and the above atmosphere modeled or observed.
Surface turbulent latent heat flux	$W \cdot m^{-2}$	The turbulent latent heat flux at the interface of ice and the above atmosphere modeled or observed.
Conductive heat flux	$W \cdot m^{-2}$	Conductive heat flux within the ice slab.
Other potential optional output parameters:		
Surface skin temperature	K	Ice/snow surface skin temperature, observed.
Surface air temperature	K	Surface air temperature at 2 m above the ground, modeled or observed.
Surface air humidity	0%~100%	Surface air humidity, relative or mixing ratio, modeled or observed.
Surface wind	$m \cdot s^{-1}$	Surface wind speed at 2 m above the ground, observed.
Sea water salinity	PPT	Sea water salinity, modeled or observed.
Sea ice salinity	PPT	Sea ice salinity, modeled or observed.
Snow depth	m	Snow accumulation over the ice in meter, modeled or observed.
Water freezing point	K	The temperature at which water freezes, modeled or observed.
Snow conductivity	$W \cdot m^{-1} \cdot K^{-1}$	Snow conductivity, modeled or observed.
Ice conductivity	$W \cdot m^{-1} \cdot K^{-1}$	Ice conductivity, modeled or observed.

Ice thickness and age quality control flags and product quality information are given in Tables 6 and 7.

Table 6. Quality Control (QC, 2 bytes).

Byte	Bit	Quality Flag Name	Description	Meaning
0	0	QC_OUTPUT	Output product quality	00 - good/optimal retrieval 01 - uncertain/suboptimal retrieval 10 - bad/missing retrieval 11 - non-retrieval
	1			
	2			
	3			
	4			
	5			
	6			
	7			

Table 7. Products Quality Information (PQI, 4 bytes)*.

Byte	Bit	Quality Flag Name	Description	Meaning
0	0	QC_INPUT_CLD	Cloud mask	00 - clear 01 - probably clear 10 – probably cloudy 11 - cloudy
	1			
	2	QC_INPUT_DAY	Day/Night	0-Day 1-Night
	3	QC_INPUT_SUNGLINT	Sunglint or not	0-Yes 1-No
	4	QC_INPUT_CLDSHADOW	Cloud shadow or not	0-Yes 1-No
	5	QC_INPUT_ICEIDEN	Ice identification	0-Yes 1-No
	6	QC_INPUT_ICECONC	Ice concentration	0-Yes 1-No
	7	QC_INPUT_ICETRAN	Ice transmittance	0-Yes 1-No
1	0	QC_INPUT_SOLZEN	Valid solar zenith angle	0-Yes 1-No
	1	QC_INPUT_SATZEN	Valid satellite zenith angle	0-Yes 1-No
	2	QC_INPUT_ALBEDO	Surface broadband albedo	0-Yes 1-No
	3	QC_INPUT_TSURF	Surface skin temperature	0-Yes 1-No
	4	QC_INPUT_SNOW	Surface snow depth	0-Yes 1-No
	5	QC_INPUT_WIND	Surface wind speed	0-Yes 1-No
	6	QC_INPUT_SURFACE	Surface background flag	00 - in-land water 01 - sea water 10 - land 11 - others
	7			
2	0	QC_INPUT_TAIR	Surface air temperature	0-Yes 1-No
	1	QC_INPUT_PRESSURE	Surface air pressure	

				0-Yes 1-No
	2	QC_INPUT_HUMIDITY	Surface air relative humidity	0-Yes 1-No
	3	QC_INPUT_SSWD	Surface shortwave downward radiative flux	0-Yes 1-No
	4	QC_INPUT_SLWD	Surface longwave downward radiative flux	0-Yes 1-No
	5	QC_INPUT_SLWU	Surface longwave upward radiative flux	0-Yes 1-No
	6	QC_INPUT_SSHF	Surface turbulent sensible heat flux	0-Yes 1-No
	7	QC_INPUT_SLHF	Surface turbulent latent heat flux	0-Yes 1-No
3	0	QC_INPUT_SCHF	Surface conductive heat flux	0-Yes 1-No
	1	QC_INPUT_SRHF	Surface residual heat flux	0-Yes 1-No
	2	QC_RET_ALGO	Day/Night algorithm selection	0-Day 1-Night
	3	QC_RET_METH	Math method for solution	0-Analytical 1-Numerical
	4	QC_RET_RESU	Retrieval success or fail	0-Success 1-Fail
	5			
	6			
	7			

*: The "Yes/No" flag indicates whether or not that input parameter is available. Some input parameters must be given in order to do ice thickness/age retrieval; these critical input parameters are date and time, cloud mask, land mask, solar zenith angle, surface skin temperature, ice mask and concentration. Other input parameters can be missing or unavailable for input, so-called optional able-to-missing parameters, that will result in the algorithm default values of those parameters being used or calculated by OTIM built-in parameterization schemes, those parameters include surface air temperature, humidity, pressure, and wind speed, surface broadband albedo, ice slab transmittance, cloud fraction, ice and snow thermal and optical physical properties, snow mask and depth, day/night indicator, shortwave and thermal radiation fluxes, and turbulent sensible and latent heat fluxes. Cloud shadow mask, sunglint mask, and satellite view angle are currently not required by the algorithm.

Metadata are listed in Table 8.

Table 8. Metadata included with the product.

Variable Name	**Definition**
Tot_QACat01	Number of QA flag values with Good or Optimal retrievals
Tot_QACat02	Number of QA flag values with Uncertain or Suboptimal retrievals
Tot_QACat03	Number of QA flag values with Bad or missing retrievals

Tot_QACat04	Number of QA flag values with Non-retrievable retrievals
TotWaterPixs	Number of pixels with water surface
TotRetrPixs	Number of valid ice thickness and age retrievals (good + uncertain)
TermntPixPct	Percentage of terminator pixels (Non-retrievable and Bad)
TotDaytimePixs	Number of valid daytime ice thickness and age valid retrievals
TotNighttimePixs	Number of valid nighttime ice thickness and age valid retrievals
MeanIceThk	Mean valid ice thickness retrievals
MaxIceThk	Maximum of valid ice thickness retrievals
MinIceThk	Minimum of valid ice thickness retrievals
STDIceThk	Standard Deviation of valid ice thickness retrievals

4 TEST DATA SETS AND VALIDATEION

4.1 Simulated/Proxy Input Data Sets

The simulated/proxy input data sets used to test this algorithm included APP-x, MODIS, SEVIRI observations as detailed in the following subsections.

4.1.1 APP-x Data

The Advanced Very High Resolution Radiometer (AVHRR) Polar Pathfinder (APP) project (Fowler, et al, 2002) recently produced 23 years of twice-daily, bi-polar surface temperature, surface albedo, and cloud information products. The APP data is being extended to include cloud properties and surface radiative fluxes (Wang and Key, 2003). The extended AVHRR Polar Pathfinder data set, called APP-x data set, covers entire Arctic and Antarctica area and spans 1982-2004 at a spatial resolution of 25 km. The specifically interested data in this work are its cloud information, surface skin temperature, surface broadband albedo, and surface radiation fluxes retrieved from satellite observations as inputs to the OTIM for estimating ice thickness and age along with other ancillary profile data and wind data from NCAR/NCEP. Figure 2 is an example of this algorithm retrieved monthly ice thickness and ice age with APP-x data.

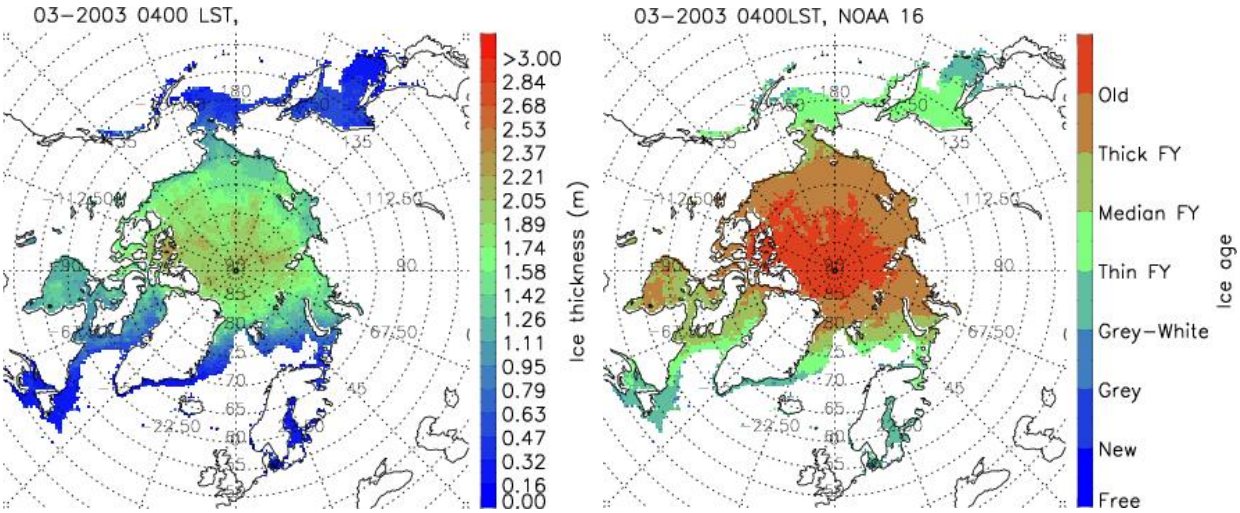

Figure 2. Retrieved monthly mean ice thickness (left) and ice age (right) with APP-x data for March 2003 under all sky condition.

4.1.2 MODIS Data

MODIS (Moderate Resolution Imaging Spectroradiometer) is a key instrument aboard the Terra (*EOS AM, refer to http://terra.nasa.gov/*) and Aqua (*EOS PM, refer to http://aqua.nasa.gov/*) satellites. Terra's orbit around the Earth is timed so that it passes from north to south across the equator in the morning, while Aqua passes south to north over the equator in the afternoon. The MODIS instrument has a viewing swath width of 2,330 km and views the entire surface of the Earth every one to two days. Its detectors measure 36 spectral bands between 0.405 and 14.385 μm, and it acquires data at three spatial resolutions that are 250m, 500m, and 1,000m. Many data products derived from MODIS observations describe features of the land, oceans and the atmosphere that can be used for studies of processes and trends on local to global scales to improve our understanding of global dynamics and processes occurring on the land, in the oceans, and in the lower atmosphere. MODIS is playing a vital role in the development of validated, global, interactive Earth system models able to predict global change accurately enough to assist policy makers in making sound decisions concerning the protection of our environment. Figure 3 and 4 show the two cases of this algorithm retrieved daily ice thickness and ice age with MODIS data.

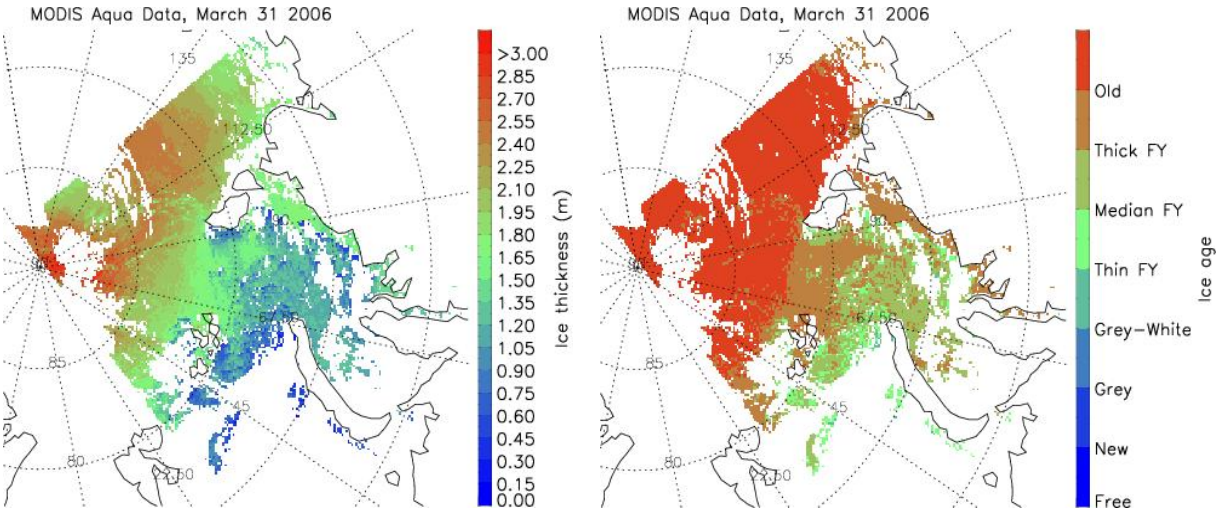

Figure 3. Retrieved ice thickness (left) and ice age (right) with MODIS Aqua data on March 31, 2006 under clear sky condition.

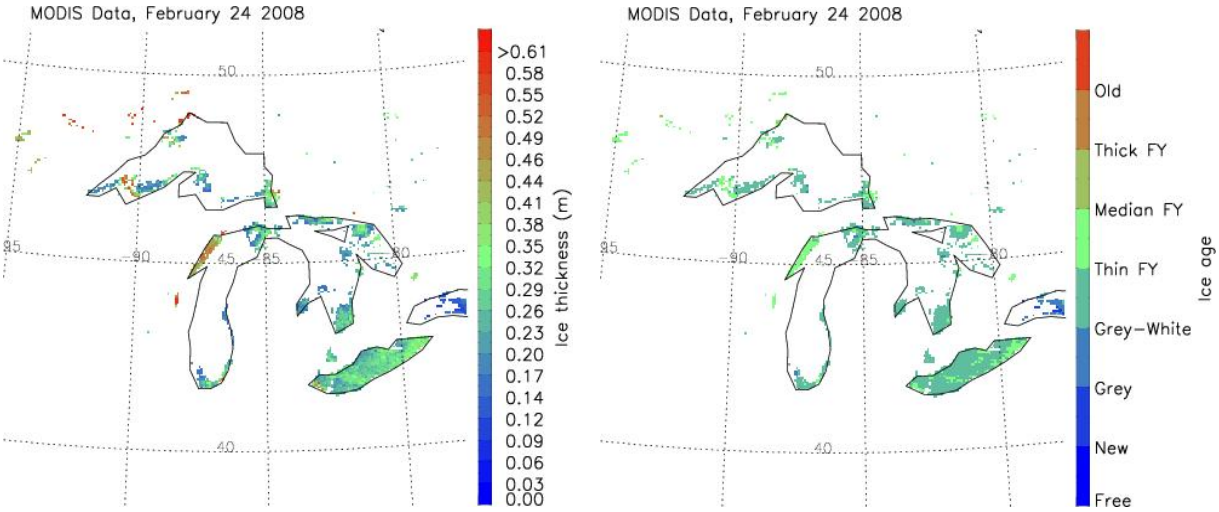

Figure 4. Retrieved ice thickness (left) and ice age (right) with MODIS Aqua data on February 24, 2008 under clear sky condition.

4.1.3 SEVIRI Data

SEVIRI (Spinning Enhanced Visible & InfraRed Imager) is the primary payload of the MSG (Meteosat Second Generation) satellites which form a joint project between the European Space Agency and Eumetsat, the European Organization for the Exploitation of Meteorological Satellites since 1977 (*refer to http://www.eumetsat.int/home/Main/Access_to_Data/Meteosat_Image_Services/SP_1123237865326*). SEVIRI measures reflected and emitted radiance in 11 spectral channels located between 0.6 μm and 14 μm with a nominal spatial resolution of 3 km at the sub-satellite point alone with an additional broadband high-resolution visible (HRV, 0.4-1.1 μm) channel that has a 1 km spatial resolution. The full disc view allows frequent sampling, every 15 minutes, enabling monitoring of rapidly evolving events. The nominal coverage includes the whole of Europe, all of Africa and locations at which the elevation to the satellite is greater than or equal to 10^{o} (Figure 5). Figure 6 shows one case of the retrieved daily ice thickness and ice age with SEVIRI data.

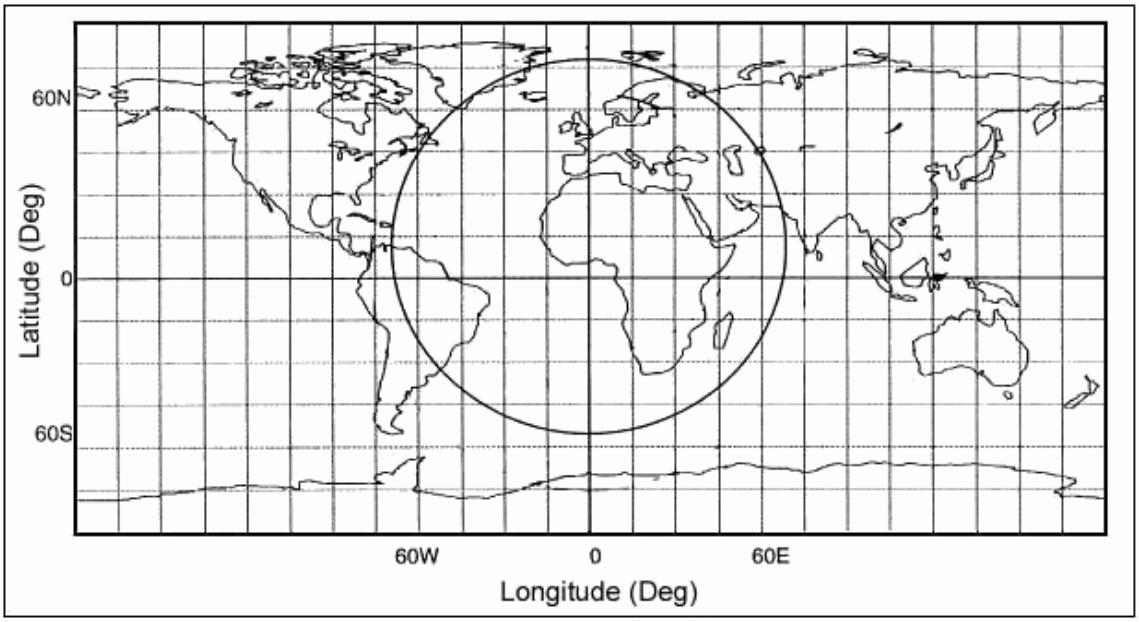

Figure 5. MSG Tele-communications coverage area.

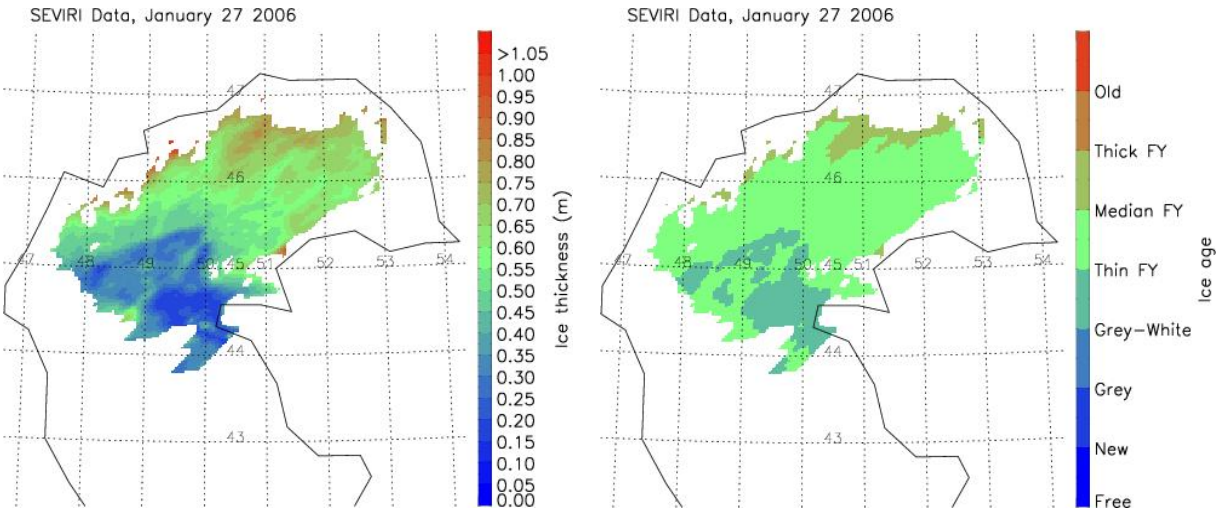

Figure 6. Retrieved ice thickness (left) and ice age (right) with SEVIRI data on January 27, 2006 under clear sky condition.

4.1.4 ABI Data

The National Oceanic and Atmospheric Administration (NOAA) Geostationary Operational Environmental Satellites (GOES)-R Series Advanced Baseline Imager (ABI) is a 16-channel imaging radiometer designed to sense radiant and solar reflected energy from Earth. It observes

the Western Hemisphere in time intervals ranging from 30 s to 15 min and at 0.5-, 1-, and 2-km spatial resolutions in visible, near-infrared (NIR), and infrared (IR) wavelengths (Schmit et al., 2005). The first satellite in the series, GOES-R, launched on November 19, 2016, and became GOES-16 when it reached geostationary orbit. Figure 7 shows one case of the retrieved daily ice thickness with GOES-R ABI data.

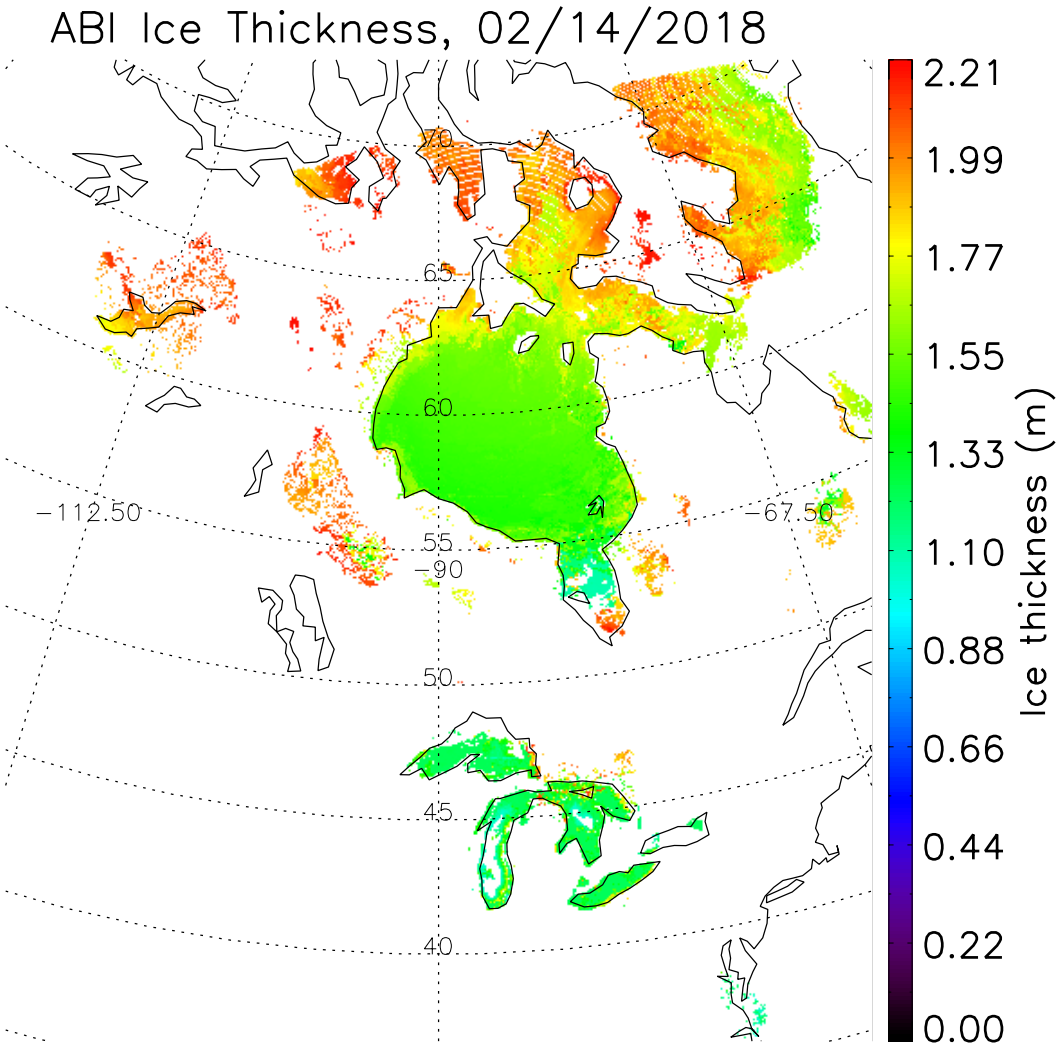

Figure 7. Retrieved daily ice thickness in Hudson Bay and Great Lakes with GOES-R ABI data on February 14, 2018 under clear sky condition.

4.1.5 VIIRS Data

The Visible Infrared Imaging Radiometer Suite (VIIRS) is a sensor designed and manufactured by the Raytheon Company on board the Suomi National Polar-orbiting Partnership (Suomi NPP) and NOAA-20 weather satellites. The VIIRS is one of five key instruments onboard Suomi NPP,

launched on October 28, 2011 that can collect imagery and radiometric measurements of the land, atmosphere, cryosphere, and oceans in the visible and infrared bands of the electromagnetic spectrum. The VIIRS has 22 imaging and radiometric bands covering wavelengths from 0.41 to 12.5 microns, providing the sensor data records for more than twenty environmental data records including clouds, sea surface temperature, ocean color, polar wind, vegetation fraction, aerosol, fire, snow and ice, vegetation. Figure 8 shows one case of the retrieved daily ice thickness with NOAA-20 VIIRS data under clear sky condition.

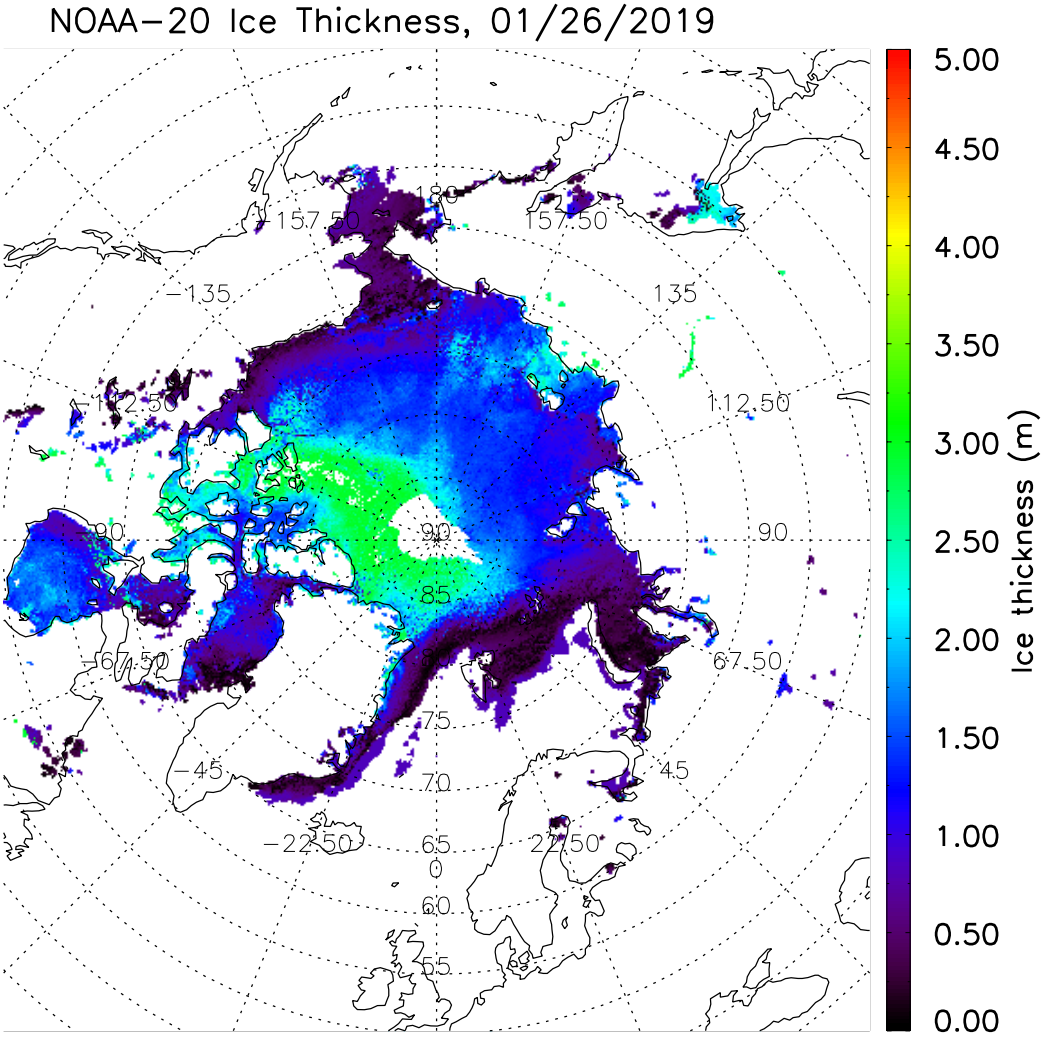

Figure 8. Retrieved daily ice thickness for the Arctic Ocean with NOAA-20 VIIRS data on January 26 2019 under clear sky conditions.

4.1.6 METimage Data

METimage is a multi-spectral (visible and IR) imaging passive radiometer which will provide detailed information on clouds, wind, aerosols and surface properties which are essential for meteorological and climate applications. METimage will provide continuity to the AVHRR (Advanced Very High Resolution Radiometer) series on board the Metop and NOAA satellites, and VIIRS on board NOAA satellites. METimage is expected to have a great improvement with respect to AVHRR and comparable performance with respect to VIIRS. The METimage measures the thermal radiance emitted by the earth and solar backscattered radiation in 20 spectral bands from 443 to 13.345 μm. Figure 9 shows one case of the retrieved overpass ice surface temperature and ice thickness with METimage proxy data from 10:23 to 12:05 UTC on September 12, 2007 under clear sky condition.

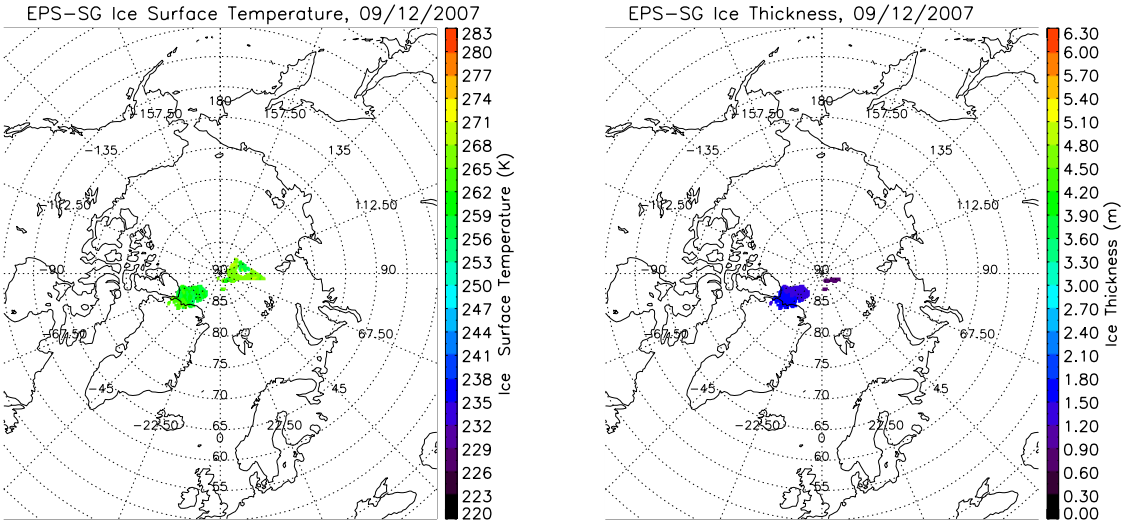

Figure 9. Retrieved one overpass ice thickness for the Arctic Ocean with METimage proxy data on September 12, 2007 under clear sky conditions.

4.2 Output from Simulated Input Data Sets

The output results from real and proxy data with this algorithm are given in the Figure 2- 4, and 6-9 in the previous section.

4.2.1 Precisions and Accuracy Estimates

To estimate the performance of this algorithm, we have used the comprehensive numerical model simulations, submarine and moored Upward Looking Sonar (ULP) measurements, and meteorological station measurements to assess and validate this algorithm. This section will present our analysis methodology for estimating the precision and accuracy. The next section will provide the quantitative results in terms of the MRD specifications.

4.2.1.1 Numerical Model Simulation Analysis

A Pan-Arctic Ice-Ocean Modeling and Assimilation System (PIOMAS) was used for this project for validation purpose. PIOMAS is a coupled Parallel Ocean and sea Ice Model (POIM, Zhang and Rothrock 2003) with capabilities of assimilating ice concentration and velocity data. It is formulated in a generalized orthogonal curvilinear coordinate (GOCC) system and designed to run on computers with a single processor or massively parallel processors. PIOMAS couples the Parallel Ocean Program (POP) with a thickness and enthalpy distribution (TED) sea-ice model. The POP model is developed at the Los Alamos National Laboratory. And the TED sea-ice model is a dynamic thermodynamic model that also explicitly simulates sea-ice ridging. The model originates from the Thorndike et al. (1975) thickness distribution theory and is recently enriched by enthalpy distribution theory (Zhang and Rothrock, 2001).

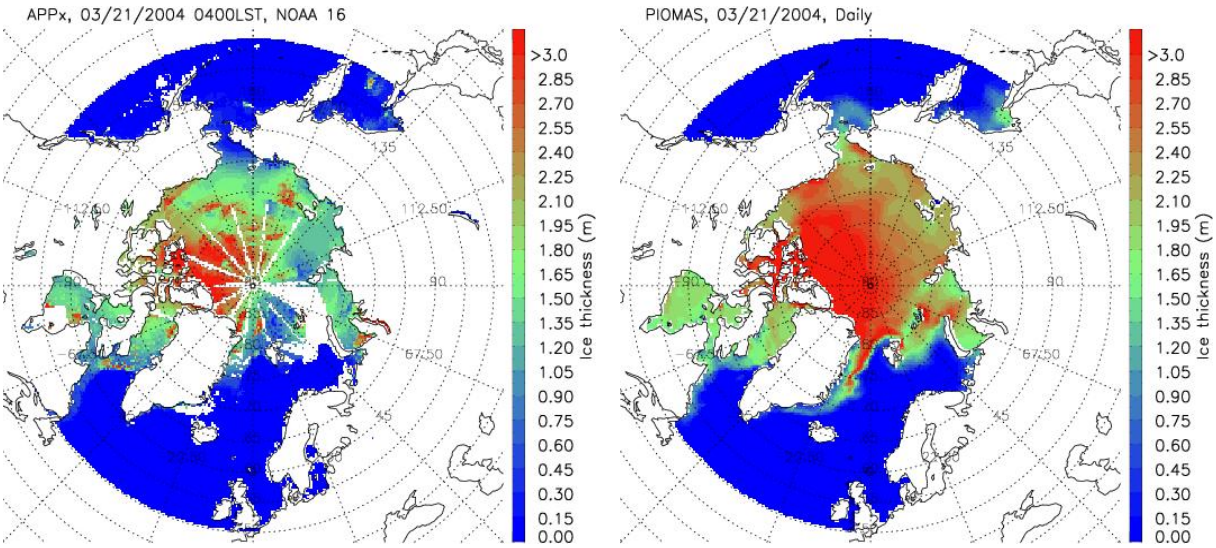

Figure 10. Retrieved ice thickness (left) with APP-x data and PIOMAS simulated ice thickness (right) for March 21, 2004 under all sky condition.

The PIOMAS data sets from the retrospective investigation include model output for 1978-2005. The outputs from the Pan-Arctic Ice-Ocean Modeling and Assimilation System (PIOMAS) provide estimates of some key ice and ocean variables. The data sets only include results for the period of 1978-2005 when satellite ice concentration data are available for assimilation. These data sets include Arctic sea ice thickness and concentration, snow depth, ice growth rate, ocean surface salinity, and others. Of special interest of this work is the PIOMAS estimated sea ice thickness. Figure 10 shows this algorithm estimated Arctic sea ice thickness with APP-x data and the PIOMAS estimation on the same day March 21 2004. Overall this algorithm estimated sea ice is thinner than PIOMAS, the inconsistence or mismatch will be investigated in the next section with submarine cruise measurements and in-situ station measurements.

4.2.1.2 Submarine Cruise Measurement Analysis

National Snow and Ice Data Center (NSIDC) archives data come from Submarine Upward Looking Sonar Ice Draft Profile Data and Statistics over past decades. This data set consists of upward looking sonar draft data collected by submarines in the Arctic Ocean. It includes data from both U.S. Navy and Royal Navy submarines. Data are provided as ice draft profiles and as statistics derived from the profile data. Statistics files include information concerning ice draft characteristics, keels, level ice, leads, undeformed and deformed ice (refer to http://nsidc.org/data/g01360.html). This data set includes submarine data collected in the Arctic Ocean by U.S. Navy and Royal Navy submarines. U.S. Navy guidance has stated that previously classified, submarine-collected ice draft data may be declassified and released according to set guidelines. Those guidelines include restrictions stating that positions of the data must be rounded to the nearest 5 minutes of latitude and longitude, and date is to be rounded to the nearest third of a month. Due to the limitations enforced by those guidelines for temporal and spatial information, not all of the data are suitable to be used by scientific study.

A program called Scientific Ice Expeditions (SCICEX) used U.S. Navy submarine for research. SCICEX data are not classified and do not have restrictions on reporting the precise location and date for the data; therefore the SCICEX ice draft data in this collection are reported with their date of acquisition, and position is reported to six decimal places, which make the SCICEX data suitable for scientific study (Figure 11). We used SCICEX 1999 ice draft data (hereafter SCICEX-99) in this work because NSIDC obtained permission to release some SCICEX-99 data acquired outside the previously mentioned release box, meaning larger area coverage for the data set. Data are in two types of files, one for ice draft profiles, and the other for statistics derived from the profile data. Ice draft files include a header that gives date and location information followed by a sequential list of drafts spaced at 1.0 m intervals that comprise the bottom-side sea-ice roughness profile. Data in each file fall along a straight-line (great circle) track between the two end points given in the header. The length of the profile in any given file can be up to 50 km, but may be shorter if data dropouts create gaps greater than 0.25 km, or if changes in course cause deviations from a straight-line track. Statistics files include information on ice draft characteristics, keels, level ice, leads, un-deformed, and deformed ice.

Figure 12 and 13 show the comparisons of the three data sets from APP-x, submarine, and PIOMAS in ice thickness. Results are given in Table 9. Note the submarine actually measures ice draft (ice below the surface), which is roughly 89% of the total ice thickness. Draft can be approximately converted to thickness with an empirical multiplicative factor of 1.1.

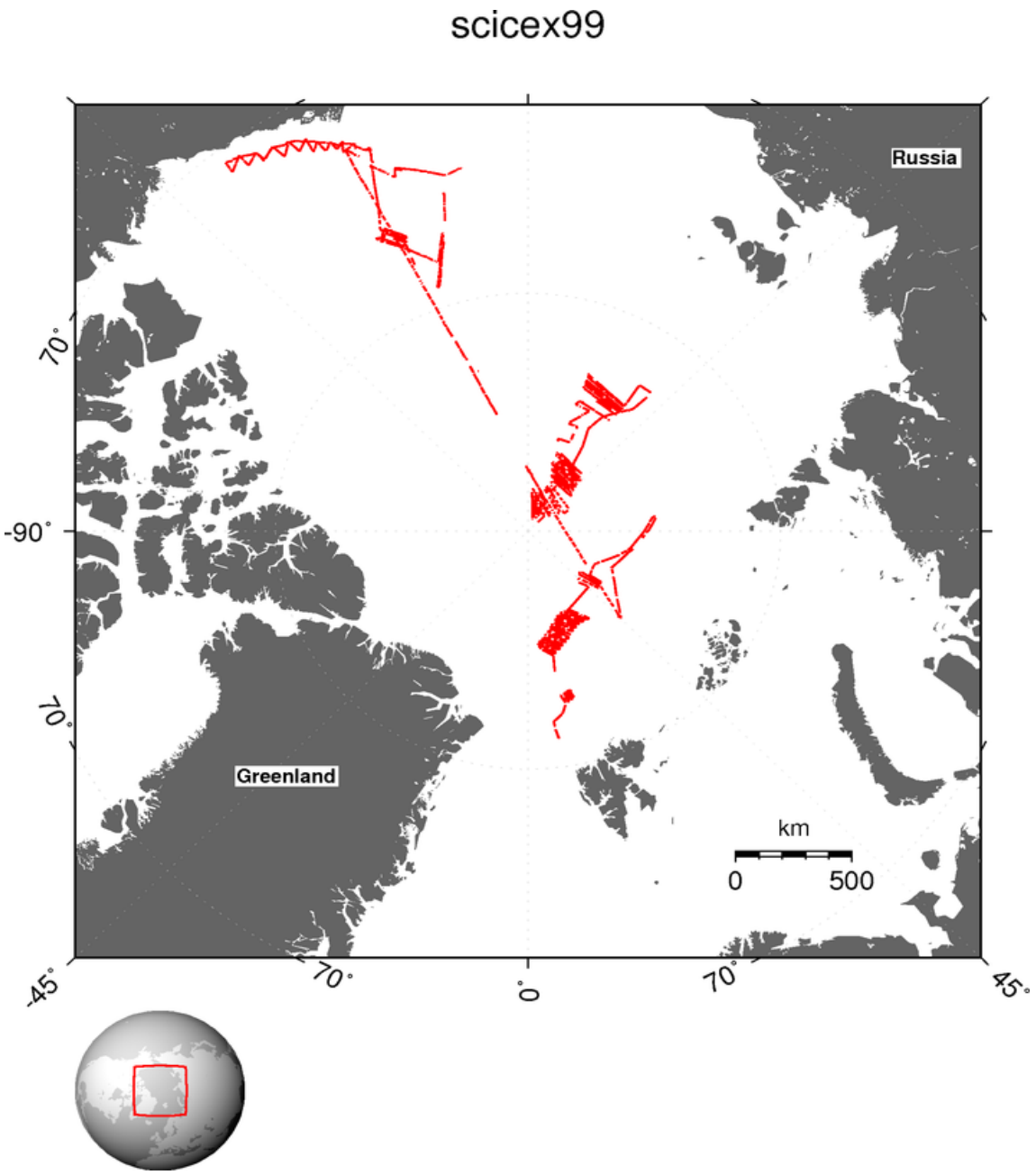

Figure 11. U.S. Navy submarine track for SCICEX ice draft data collection during April 2 – May 13 in 1999.

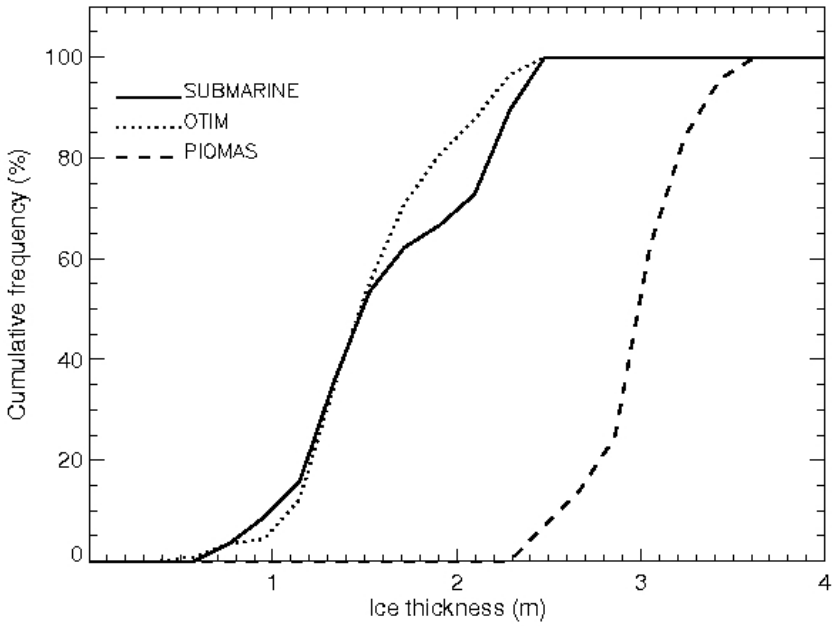

Figure 12. Comparisons of ice thickness cumulative distribution retrieved by OTIM with APP-x data, measured by submarine, and simulated by numerical model PIOMAS. Submarine ice draft (mean and median only) was already converted to ice thickness by a factor of 1.11.

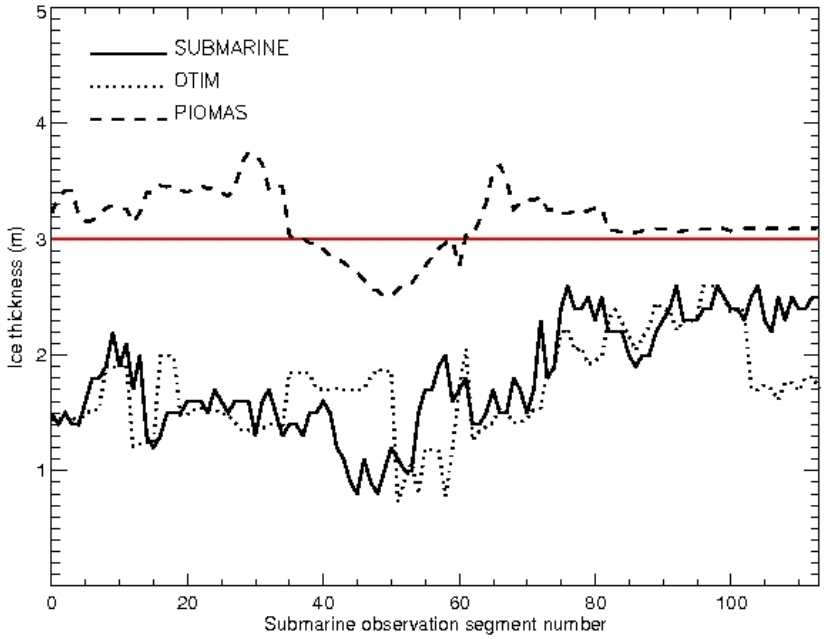

Figure 13. Comparisons of ice thickness values retrieved by OTIM with APP-x data, measured by submarine, and simulated by numerical model PIOMAS alone the submarine track segments. Submarine ice draft (mean and median only) was already converted to ice thickness by a factor of 1.11.

Table 9. Validation result against submarine measurements.

	This algorithm	Submarine
Thickness Mean (m)	1.73	1.80
Bias Mean (m)	-0.07	
Bias Absolute Mean (m)	0.31	
Bias Standard Deviation	0.42	
Accuracy*	83%	
Ice Age	Ice free water, new/fresh, nilas, grey, grey-white, first year thin, first year medium, first year thick, and multi-year ice.	
ADR Requirements	Distinguish between ice free areas, first-year ice, and older ice.	
CDR Requirements	Distinguish between Ice free, new/fresh ice, nilas, grey white, first Year medium, first Year Thick, second year, and multiyear smooth and deformed ice.	

***** *Accuracy=(1.0 – (Bias Absolute Mean)/(Submarine Mean Ice thickness))*%*

4.2.1.3 Station Measurement Analysis

The Canadian Ice Service (CIS) maintains archived Ice Thickness and On-Ice Snow Depth Measurements for Canadian Stations (Figure 14) back as far as 1947 for the first established stations in the Canadian Arctic (Eureka and Resolute). By the beginning of 2002 most stations from the original Ice Thickness program had stopped taking measurements. Fortunately, due to an increasing interest in updating this historical dataset to support climate change studies a new program was started in the fall of 2002, called New Arctic Program starting from 2002 (refer to http://ice-glaces.ec.gc.ca/App/WsvPageDsp.cfm?Lang=eng&lnid=5&ScndLvl=no&ID=11703). Several stations in the Canadian Arctic were re-opened and started taking measurements. These New Arctic Program stations are listed in Table 10. The New Arctic Program Data will be used in this work.

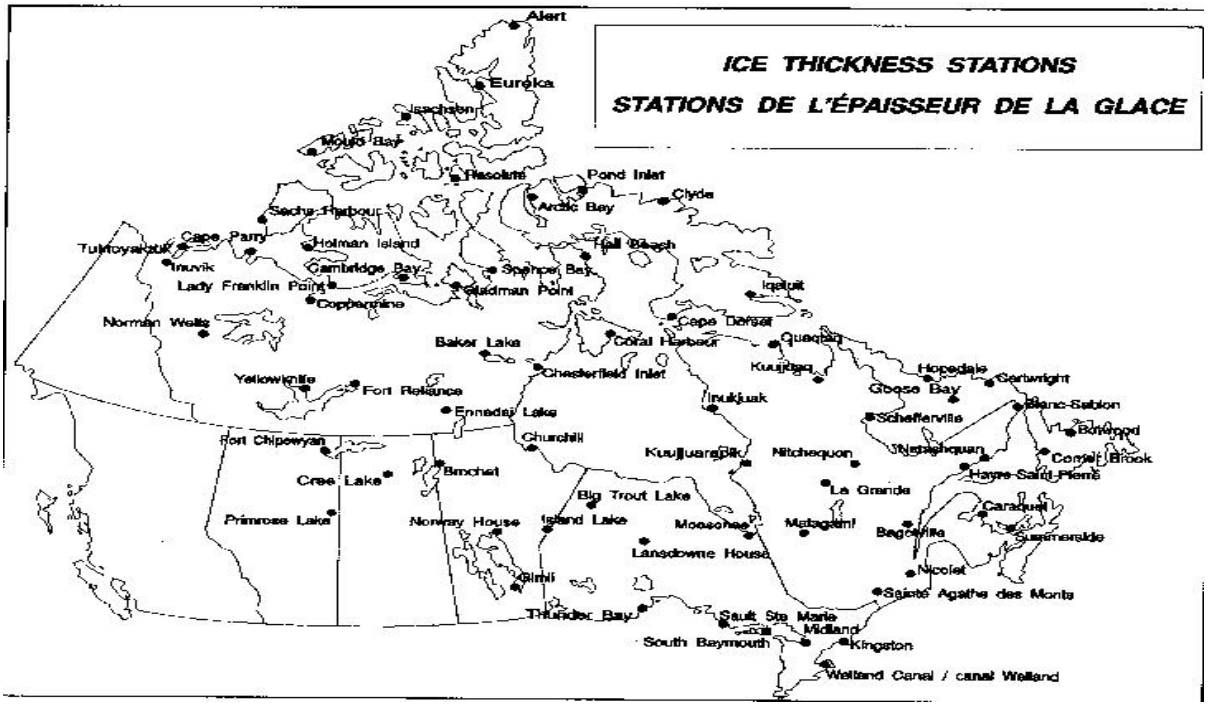

Figure 14. Spatial deployment of the Canadian stations for ice thickness and on-ice snow depth measurements.

Table 10. Geographic Information of the New Arctic Program Stations (Starting Fall 2002) for Ice Thickness and On-Ice Snow Depth Measurements.

Station ID	Station Name	Start Date	LAT	LON
LT1	ALERT LT1	10/16/2002	82.466667	-61.5
YLT	ALERT YLT	10/16/2002	82.500275	-61.716667
YBK	BAKER LAKE YBK	11/27/2002	64.316666	-95.966667
YCB	CAMBRIDGE BAY YCB	12/07/2002	69.10833	-104.95
YZS	CORAL HARBOUR YZS	11/15/2002	64.119446	-82.741669
WEU	EUREKA WEU	10/11/2002	79.986115	-84.099998
YUX	HALL BEACH YUX	11/10/2002	68.765274	-80.791664
YEV	INUVIK YEV	11/29/2002	68.35833	-132.26138
YFB	IQALUIT YFB	01/04/2003	63.727779	-67.48333
YRB	RESOLUTE YRB	12/13/2002	74.676941	-93.131668
YZF	YELLOWKNIFE YZF	11/29/2002	62.465556	-114.36556

Most of the data in the current archive at the Canadian Ice Service have been collected by the Atmospheric Environment Program of Environment Canada, but some data are provided by other organizations such as the St-Lawrence Seaway Authority, Trent University and Queen's University. Measurements are taken approximately at the same location every year on a weekly basis starting after freeze-up when the ice is safe to walk on, and continuing until break-up or when the ice becomes unsafe. The location is selected close to shore, but over a depth of water which will exceed the maximum ice thickness. Ice thickness is measured to the nearest centimeter using either a special auger kit or a hot wire ice thickness gauge. The depth of snow on the ice at the location of ice thickness measurement is also measured and reported to the nearest centimeter. Measurements after 1982 include additional information (coded values as per code for additional information at bottom) such as character of ice surface, water features and method of observation. Figures 15 and 16 show the comparisons of the three data sets for ice thickness in cumulative frequency and in absolute magnitude, respectively. Results are given in Table 11.

Table 11. Validation result against in-situ station measurements.

ALGO* Station	**AlGO ALERT LT1**	**ALGO ALERT YLT**	**ALGO CAMBRIDGE BAY YCB**	**ALGO CORAL HARBOUR YZS**	**ALGO EUREKA WEU**	**ALGO HALL BEACH YUX**	**ALGO RESOLUTE YRB**	**ALGO YELLOW KNIFE YZF**
Thickness Mean (m)	1.17 1.23	1.21 1.26	1.48 1.51	1.17 1.20	1.36 1.54	1.37 1.46	1.21 1.50	0.91 0.93
Bias Mean (m)	-0.06	-0.06	-0.04	-0.03	-0.18	-0.07	-0.29	-0.01
Bias absolute Mean (m)	0.14	0.16	0.58	0.32	0.27	0.32	0.31	0.31
Ice Age	Ice free water, new/fresh, nilas, grey, grey-white, first year thin, first year medium, first year thick, and multi-year ice.							
ADR Requirements	Distinguish between ice free areas, first-year ice, and older ice.							
CDR Requirements	Distinguish between Ice free, new/fresh ice, nilas, grey white, first Year medium, first Year Thick, second year, and multiyear smooth and deformed ice.							

* ALGO means this algorithm.

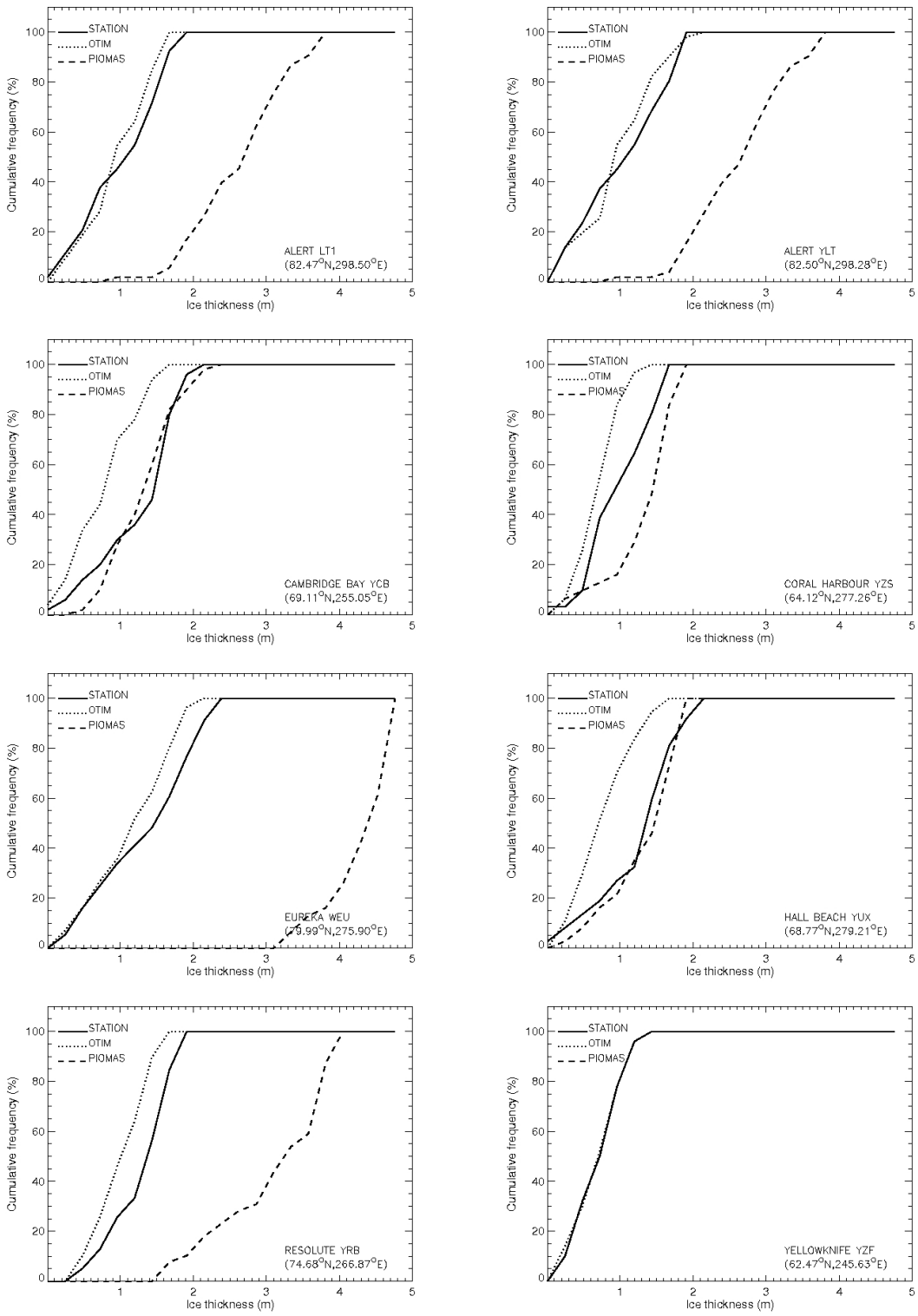

Figure 15. Comparisons of ice thickness cumulative distribution retrieved by OTIM with APP-x data, measured by stations, and simulated by numerical model PIOMAS for some locations as shown in the lower-right corner of the plot.

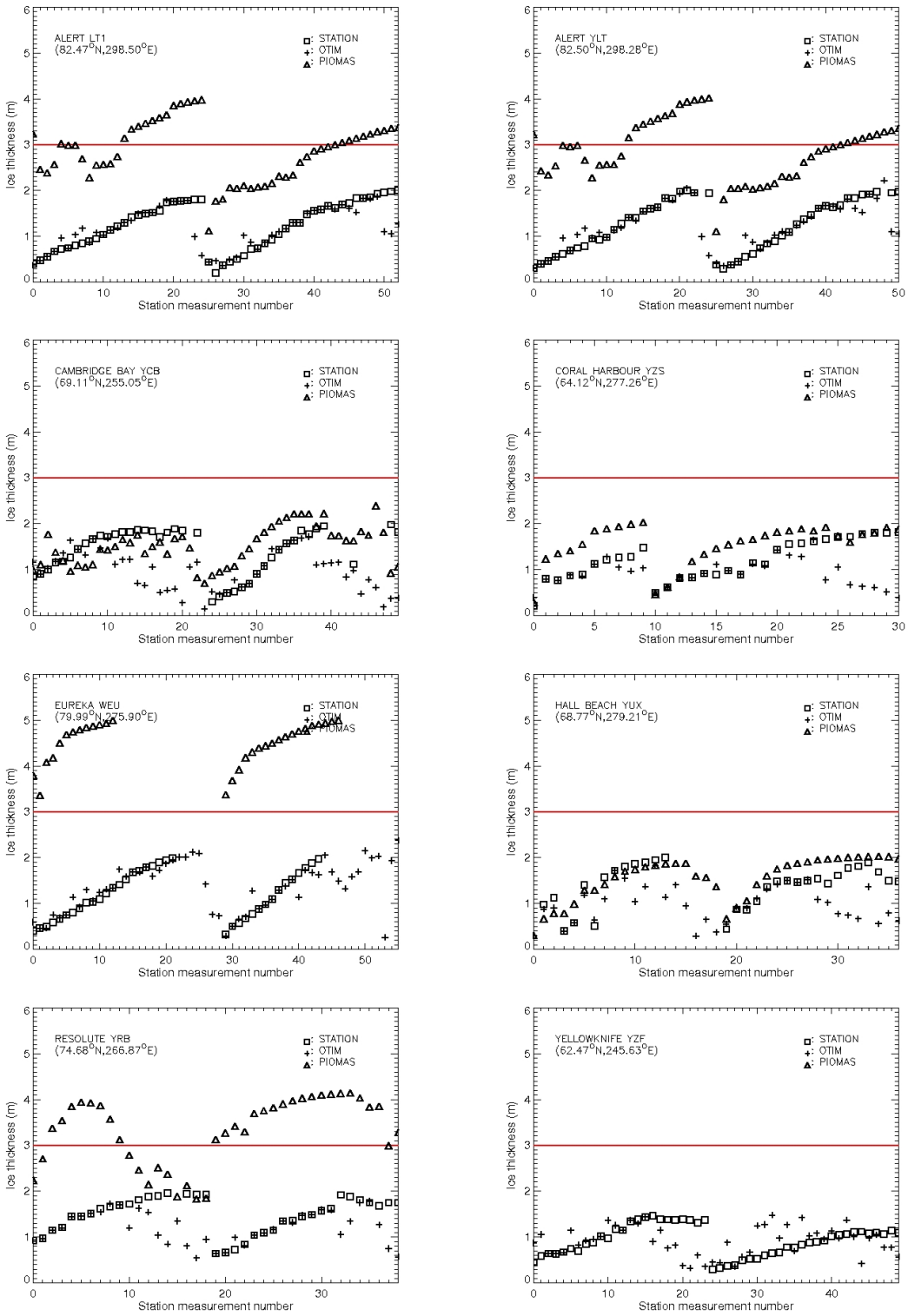

Figure 16. Comparisons of ice thickness values retrieved by OTIM with APP-x data, measured by stations, and simulated by numerical model PIOMAS at the station locations as shown in the lower-right corner of the plot.

4.2.1.4 Mooring Measurement Analysis

There are ice draft mooring data from Beaufort Gyre Exploration Project (BGEP; http://www.whoi.edu/beaufortgyre/index.html) from 2003 up to the present at three mooring sites in the Beaufort Sea area. Since 2003, Upward Looking Sonars (ULS) were deployed beneath the Arctic ice pack on Beaufort Gyre Observing System (BGOS; http://www.whoi.edu/beaufortgyre) bottom-tethered moorings (Ostrom et al., 2004; Kemp et al., 2005). Over 15 million observations are acquired for every mooring location in each year. Detailed ULS data processing can be found at http://www.whoi.edu/beaufortgyre/pdfs/BGOS%20ULS%20Data%20Processing%20Procedure.pdf. We used ice draft mooring data from 2003 and 2004 from three mooring sites because of no APP-x data available beyond 2004. The mooring ice draft is converted to ice thickness by multiplying a factor of 1.11 as the same process for submarine ice draft. The daily mean ice draft mooring data from 2003 to 2004 were used in the comparison, excluding the data from May through August due to the non-retrievals of OTIM for polar day period.

Table 12 lists mooring sites location information, time period, and comparison statistical results. Figure 17 and 18 show the comparisons of the three data sets, i.e., OTIM using APP-x, PIOMAS simulations, and mooring measurements at three sites, as a cumulative frequency ice thickness distribution and as point-to-point comparisons. Table 12 gives the statistical results of ice thickness from OTIM and from mooring measurements for all 3 sites when both of them have valid ice thickness data. The overall error is comparable to the error of OTIM against submarine and station measurements.

Table 12. The OTIM validation results against mooring measurements over 2003-2004.

Mooring Location OTIM	Thickness mean (m)	Bias mean (m)	Bias absolute mean (m)
Site A (75º0.499'N, 149º58.660'W) OTIM	1.24 1.22	-0.02 (-1.2%)	0.19 (15.3%)
Site B (78º1.490'N, 149º49.203'W) OTIM	1.32 1.17	-0.15 (-11.4%)	0.29(21.9%)
Site C (76º59.232'N, 139º54.562'W) OTIM	1.32 1.20	-0.12 (-9.1%)	0.28 (21.2%)
ALL MOORING AVERAGE OTIM AVERAGE	1.29 1.20	-0.09 (-6.9%)	0.25 (19.4%)

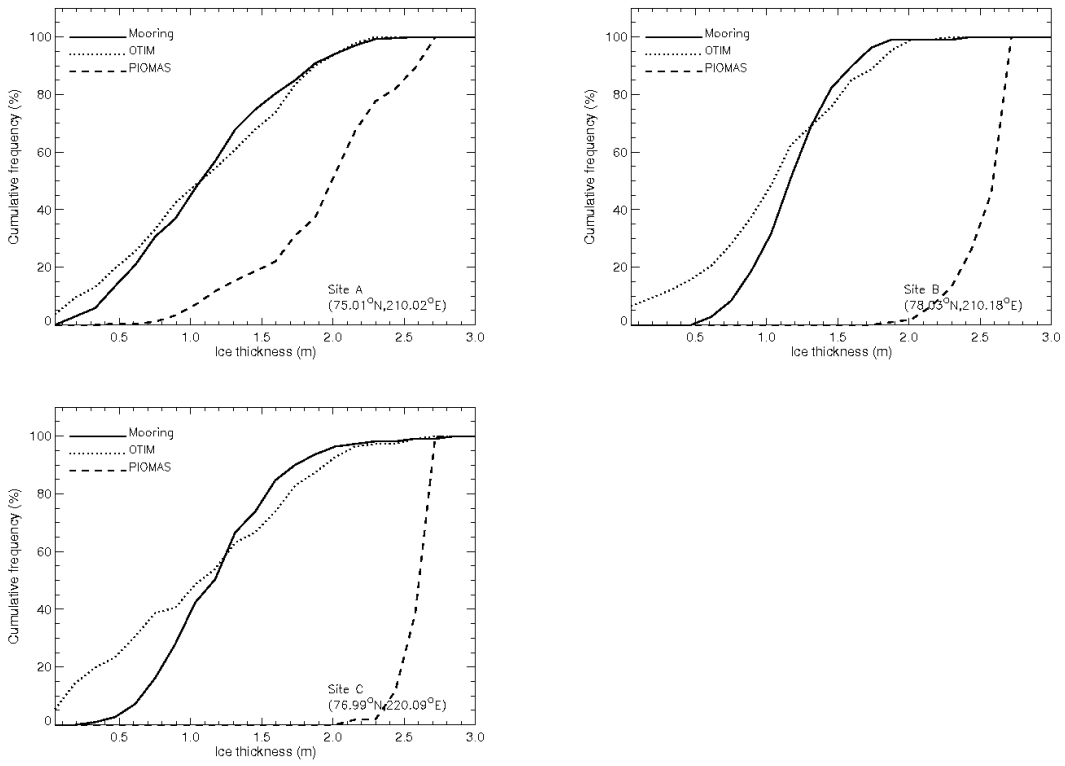

Figure 17. Comparisons of ice thickness cumulative distribution retrieved by OTIM with APP-x data, simulated ice thickness from the PIOMAS model and the ULS measurements at the mooring sites A, B, and C.

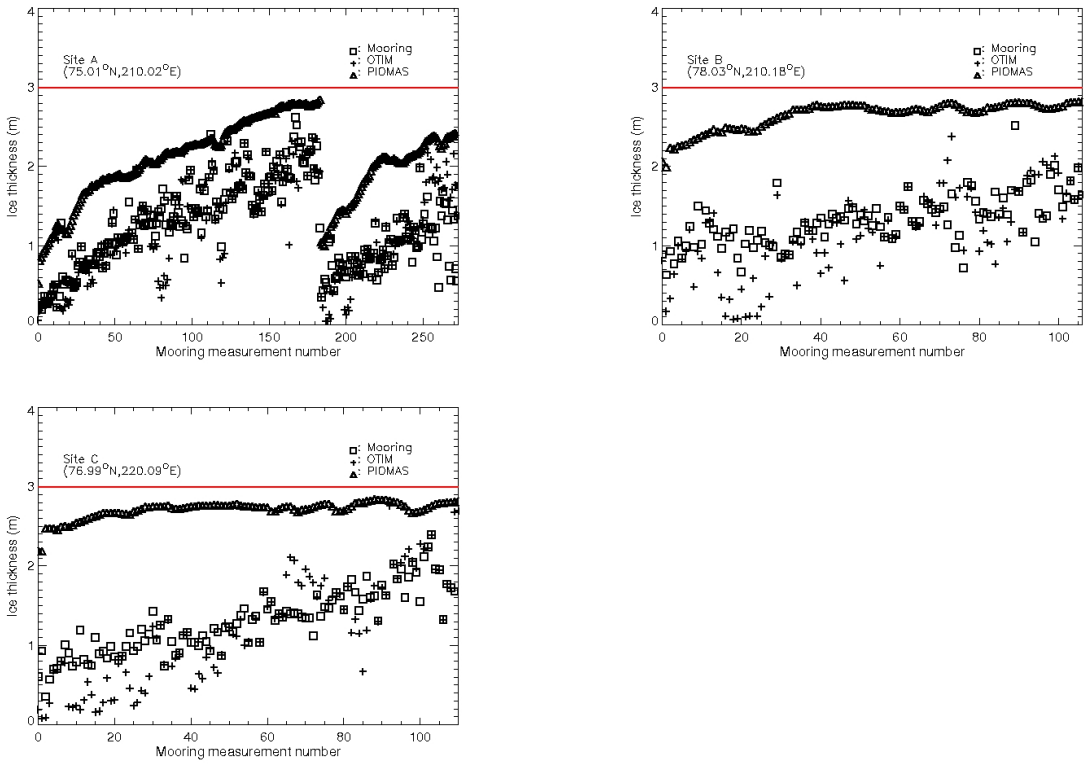

Figure 18. Comparisons of ice thickness values retrieved by OTIM with APP-x data, ULS measured ice thickness at the mooring site A, and simulated ice thickness from the PIOMAS model.

4.2.1.5 Microwave Data Derived Ice Age Analysis

There is a data set of sea ice concentrations (the fraction, or percentage, of ocean area covered by sea ice) available at http://nsidc.org/data/nsidc-0051.html. This data set is generated from brightness temperature data derived from Nimbus-7 Scanning Multichannel Microwave Radiometer (SMMR) and Defense Meteorological Satellite Program (DMSP) -F8, -F11 and -F13 Special Sensor Microwave/Imager (SSM/I) radiances at a grid cell size of 25 x 25 km. These data include gridded daily (every other day for SMMR data) and monthly averaged sea ice concentrations for both the north and south polar regions. The data are generated using the NASA Team algorithm developed by the Oceans and Ice Branch, Laboratory for Hydrospheric Processes at NASA Goddard Space Flight Center (GSFC), and include data since 26 October 1978. Final data are produced from SMMR brightness temperature data processed at NASA GSFC and SSM/I brightness temperature data processed at the National Snow and Ice Data Center (NSIDC). These sea ice concentration data from passive microwave observations were used as a independent validation data resource for ice age product. We used this microwave sea ice concentration data to derive sea ice age in the Arctic Ocean, i.e., ice free, first-year ice, and older ice by tracking daily sea ice concentration for each pixel over a year-long period. If an areal Sea Ice Concentration (SIC) is less than 15% all the year round on any day, it is identified ice free area, if only for certain period of time over a year, it is identified as first-year ice area,

and if the areal SIC is never less than 15% on any day for a year, it is identified older ice area. The ice age product derived from passive microwave data this way is reckoned ice age proxy truth.

We collected 2412 data granules covering the Arctic from MODIS Terra and Aqua for March, 2006, and applied our algorithm to derive ice age product, and then composed all those MODIS granules to form a fully covered Arctic ice age map for the comparison with microwave derived ice age truth. Figure 19 shows MODIS derived ice age (middle) with our algorithm from a composite of Terra & Aqua MODIS data in March, 2006, and the ice age (left) derived from microwave ice concentration (NASA team algorithm) data using a tracking method over the year 2006. Inaccuracies in the MODIS cloud mask can severely affect the accuracy of ice thickness and age products. The performance of our ice age product algorithm is assessed by performance metrics of product accuracy and precision. The product accuracy is defined as the percentage ratio of the OTIM retrieval against truth, and the product precision is defined as the standard deviation of the errors between OTIM retrievals and truth. Tables 13, 14, and 15 list the statistical results between OTIM retrieval and truth in terms of total number of pixels in each category of ice free, first-year ice, and older ice, product accuracy, and product precision. As seen, overall our algorithm derived ice age product fulfills the requirements of 80% product accuracy and less than one category product precision. MODIS daytime data seems to have higher product accuracy and precision. That is due to the very few daytime data (small samples) available from MODIS Terra & Aqua for the Arctic Ocean in March 2006, and the most part of Arctic Ocean are in dark around the clock in winter.

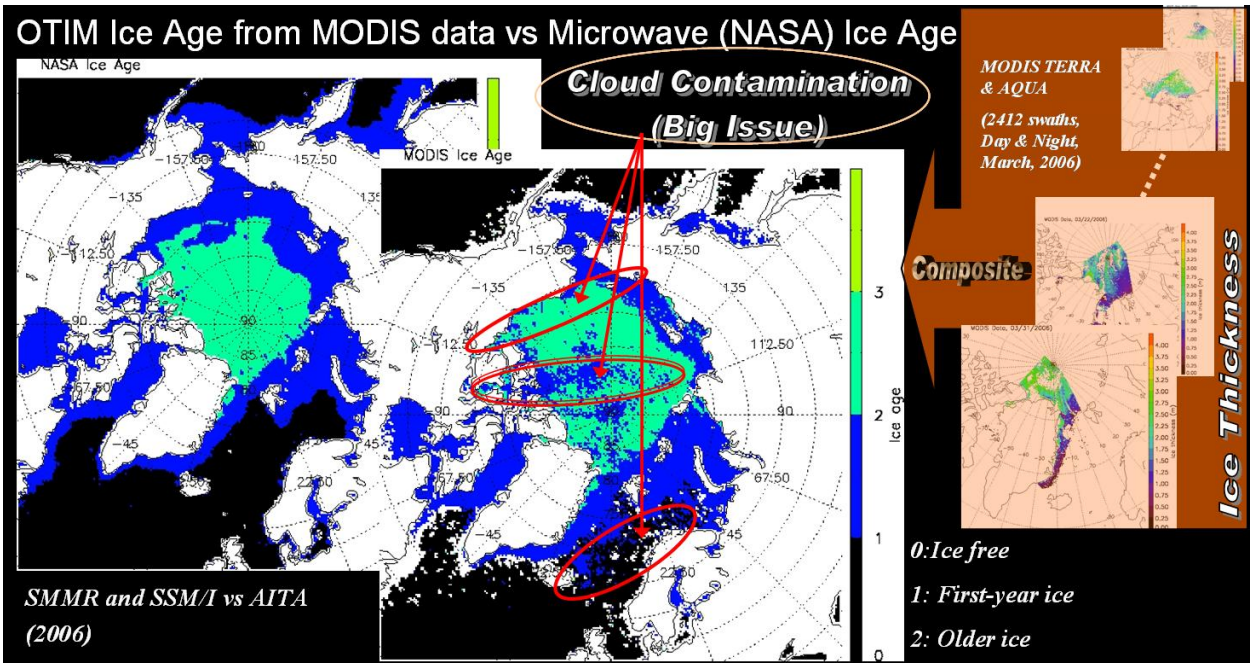

Figure 19. Sensitivity of ice thickness to expected uncertainties in the controlling variables for daytime case with reference ice thickness of 0.3 (red), 1 (black), and 1.8 (blue) meters.

Table 13. The statistical matrix of the comparison in ice age between OTIM derived ice age with MODIS data and NASA team algorithm derived ice age with passive microwave data.

Note: Number in each cell stands for the number of pixels that belong to the ice age categories corresponding to NASA and OTIM ice age classifications used to do statistics, i.e., accuracy and precision in ice age classification.		**NASA Ice Age Truth***			
		Ice Free	**First-year Ice**	**Older Ice**	**Total**
OTIM Ice Age This Study)	**Ice Free**	***(D&N:32278) (N:32288) (D:34681)***	***(D&N:0) (N:0) (D:0)***	***(D&N:0) (N:0) (D:0)***	**(D&N:32278) (N:32288) (D:34681)**
	First-year Ice	***(D&N:2381) (N:2371) (D:30)***	***(D&N:12623) (N:12615) (D:93)***	***(D&N:1141) (N:1141) (D:0)***	**(D&N:16145) (N:16127) (D:123)**
	Older Ice	***(D&N:52) (N:52) (D:0)***	***(D&N:2632) (N:2634) (D:0)***	***(D&N:5919) (N:5919) (D:0)***	**(D&N:8603) (N:8605) (D:0)**
	Total	**(D&N:34711) (N:34711) (D:34711)**	**(D&N:15255) (N:15249) (D:93)**	**(D&N:7060) (N:7060) (D:0)**	**(D&N:57026) (N:57020) (D:34804)**

* D=Day, N=Night, D&N=Day and Night

Table 14. The statistical results in terms of product accuracy for the comparison in ice age between OTIM derived ice age with MODIS data and NASA team algorithm derived ice age with passive microwave data.

Ice Age (OTIM vs Microwave)*	
Statistics	**Accuracy!**
Ice Free	D&N:93%, N:93%, D:~100%
First-year Ice	D&N:92%, N:92%, D:~100%
Older Ice	D&N:84%, N:84%, D:~100%
All	D&N:89%, N:89%, D:~100%
Error Sources	1. *Ice identification algorithm* 2. *Cloud mask/shadow detection* 3. *Relationship between thickness and age* 4. *Ice motion/Dynamic processes*

* D=Day, N=Night, D&N=Day and Night

Table 15. The statistical results in terms of product precision for the comparison in ice age between OTIM derived ice age with MODIS data and NASA team algorithm derived ice age with passive microwave data.

Note: Number in each cell stands for the number of pixels that belong to the ice age category difference corresponding to NASA and OTIM ice age classifications used to do statistics, i.e., accuracy and precision in ice age classification.	**Ice Age Difference (OTIM vs Microwave)**		
	No Difference	**1 Category Difference**	**2 Category Difference**
	(D&N:49820) (N:49822) (D:34774)	(D&N:7154) (N:7146) (D:30)	(D&N:52) (N:52) (D:0)
Precision	**(D&N:0.34 Category)** **(N:0.34 Category)** **(D:0.03 Category)**		

* D=Day, N=Night, D&N=Day and Night

4.2.2 Error Budget

In estimation of ice thickness by using the OTIM, many factors affect the accuracy of ice thickness. The uncertainties from all of the input controlling variables in the OTIM will finally propagate into ice thickness through the ways of parameterizations and model algorithms. Theoretically and mathematically speaking, we can describe the estimate of ice thickness as a function of heat fluxes and surface albedo and transmittance:

$$\hat{h}_i = f(\hat{\alpha}_s, \hat{i}_0, \hat{F}_r, \hat{F}_l^{up}, \hat{F}_l^{dn}, \hat{F}_s, \hat{F}_e, \hat{F}_c, \hat{F}_a) \qquad (31)$$

where the variables with carets "^" are the variables defined in Equation (1). In the OTIM model we used parameterization schemes (Key et al, 1996) as described in previous sections to calculate $\hat{F}_l^{up}, \hat{F}_l^{dn}, \hat{F}_s, \hat{F}_e, \hat{F}_c$, all of which are functions of surface skin and air temperatures (***T_s*, *T_a***), surface air pressure (P_a), surface air relative humidity (R), ice temperature (T_i), wind speed (U), cloud amount (C), and snow depth (h_s), therefore ice thickness is actually the function of those variables expressed in Equation (32):

$$\hat{h}_i = f(\hat{\alpha}_s, \hat{i}_0, \hat{F}_r, \hat{T}_s, \hat{T}_i, \hat{T}_a, \hat{P}_a, \hat{R}, \hat{U}, \hat{C}, \hat{h}_s, \hat{F}_a) \qquad (32).$$

Suppose the true ice thickness h_i is estimated from the true values of all controlling variables in the Equation (32), and let x_i represent the variables in equation (32) with true values, and $\hat{x}_i$ represent those variable with estimated values, and *x's* subscript *i* is from 1 to 12 representing 12 variables in the Equation (32), thus if the uncertainties in the controlling variables are

independent and random, the statistics of the error $(\hat{h}_i - h_i)$ can be expressed in terms of the uncertainties in the variables on which it depends:

$$(\hat{h}_i - h_i) = \sum (\hat{x}_i - x_i) \frac{\partial h_i}{\partial x_i} \qquad (33)$$

or the variance in the thickness error, as

$$\sigma_{h_i}^2 = \sum \sigma_{x_i}^2 (\frac{\partial h_i}{\partial x_i})^2 \qquad (34)$$

However, as discussed by Key et al (1997), if the variables are not independent of each other, then the covariances between them must be considered. Unfortunately, data needed to estimate the covariance between all pairs of variables are often not available. If the covariance between pairs of variables is unknown, then it can be shown (Taylor, 1982) that the total uncertainty will never exceed

$$\sigma_{h_i} \le \sum \sigma_{x_i} | \frac{\partial h_i}{\partial x_i} | \qquad (35)$$

Table 11 and 12 give estimates of the partial derivatives needed in the Equations (33), (34), and (35), computed using differences ($\Delta h_i/\Delta x_i$). These partial derivatives can be used for the calculations of the sensitivity of the ice thickness to errors in the controlling variables.

The estimated uncertainties in the controlling variables in Equation (32), e.g. surface skin temperature T_s, are now used to assess the accuracy with which ice thickness can be estimated using satellite data products. Since ice thickness vary nonlinearly with respect to the controlling variables under investigation, its sensitivity to errors varies over the range of the input controlling variables. Therefore, uncertainty in ice thickness is estimated for a set of reference values that represent the typical values for certain thick ice as listed in Table 11 and 12.

To estimate σ_{h_i}, we need to first estimate the uncertainties of all controlling variables in Equation (32). According to Wang and Key's study (2005), for the satellite retrieved surface broadband albedo α_s, the uncertainty would be as large as 0.10 in absolute magnitude that is used here. Regarding the ice slab transmittance i_0, we use absolute uncertainty of 0.05 in this study, which is kind of arbitrary and probably larger than actual value. Satellite retrieved surface downward shortwave radiation flux F_r can be biased high or low by 20% of the actual value or 35 W m^{-2} as compared with in-situ measurements (Wang and Key, 2005). Wang and Key (2005) also estimated the uncertainties in satellite-derived surface skin temperature T_s and cloud amount C with respect to the Surface Heat Balance of the Arctic Ocean (SHEBA) ship measurements (Maslanik et al., 2001) that can be as large as 2 K and 0.25 in absolute magnitude, respectively, and we take 2 K as surface air temperature T_a uncertainty as well. Since surface may be covered with a layer of snow, ice slab temperature T_i may be different from T_s, therefore assuming $T_i = T_s$ may introduce additional error in ice thickness estimation, we elect to assign 5 K uncertainty in

T_i to estimated its impact on the ice thickness since there is no known information about the difference between T_i and T_s, and Satellite can only retrieve surface skin temperature T_s, not T_i. The uncertainties in surface air pressure and relative humidity together with surface temperature will affect the ice thickness estimation indirectly through the impact of turbulent sensible and latent heat fluxes. A change of 50 *hPa* surface air pressure may induce changing weather pattern, we take 50 *hPa* as possible maximum uncertainty of surface air pressure. The uncertainty in geostrophic wind U_G could be 2 m s^{-1} as determined by the buoy pressure field (Thorndike and Colony, 1982), and the relationship $U = 0.34U_G$ gives the uncertainty in surface wind speed U of 0.7 m s^{-1}, we take 1 m s^{-1} as possible actual uncertainty in this study. An uncertainty of 10% in surface air relative humidity is adopted in this work. Snow cover directly affects conductive heat flux, surface albedo, and the radiative fluxes at the interface of the ice-snow. Snow depth h_s plays a big role, accurate and spatially wide covered measurements are usually not available coincidentally in time and space with satellite observations, and also changes over time with wind and topography. It is hard to know the uncertainty in snow depth estimation, and we think it is reasonable to give 50% of the given snow depth as its uncertainty in general. The last uncertainty source is the surface residual heat flux F_a, which is associated ice growth, ablation, and possible horizontal heat gain/loss. In the case of no melting and horizontal heat gain/loss, F_a is zero, which is widely accepted by ice models if the surface temperature is below freezing point. We set uncertainty of F_a 2 W m^{-2} as an initial guess. The overall error caused by the uncertainties in those controlling variables for ice thickness estimation may not be equal to the summation of all errors from each individual uncertainty source because the opposite effects may cancel each other among the uncertainty sources resulting in a less error as mathematically described by Equation (35).

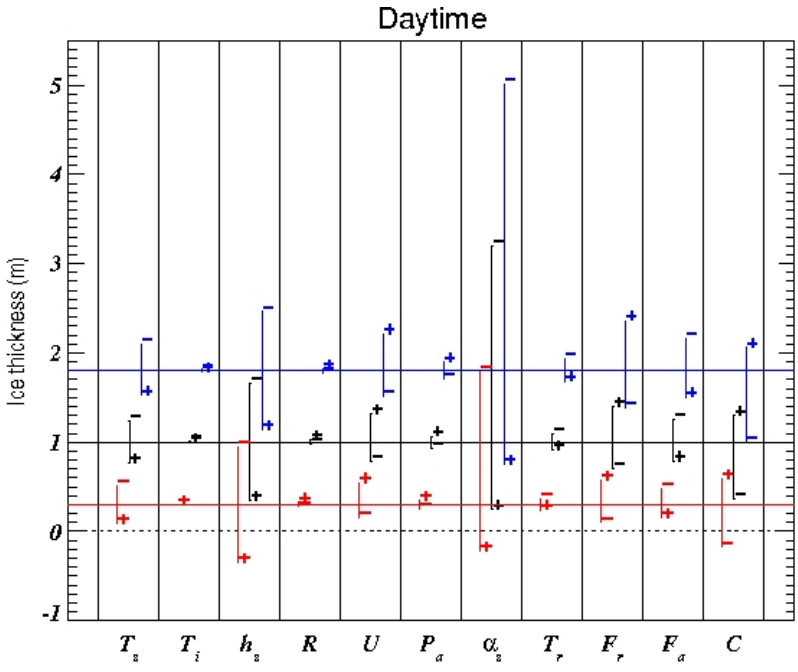

Figure 20. Sensitivity of ice thickness to expected uncertainties in the controlling variables for daytime case with reference ice thickness of 0.3 (red), 1 (black), and 1.8 (blue) meters.

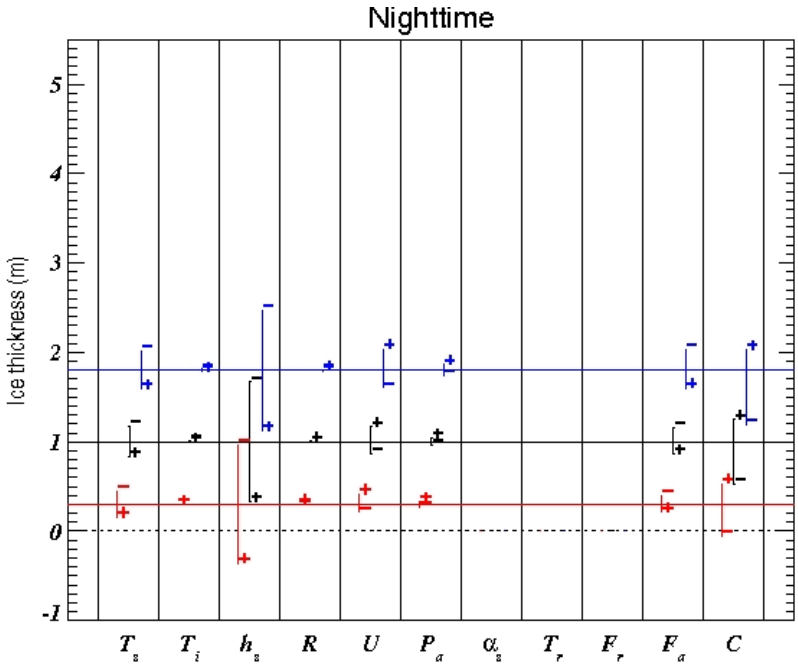

Figure 21. Sensitivity of ice thickness to expected uncertainties in the controlling variables for nighttime case with reference ice thickness of 0.3 (red), 1 (black), and 1.8 (blue) meters.

Tables 16 and 17 list the controlling variables used in ice thickness sensitivity study for daytime and nighttime cases with aforementioned uncertainties in controlling variables and their impacts for typical ice thickness of 1 meter. The results of this sensitivity study are shown graphically in Figures 20 and 21 based on the reference ice thickness values of 0.3, 1.0, 1.8 meters with those expected uncertainties in controlling variables. The bars give the overall range in the ice thickness corresponding to the uncertainties listed in the Tables 16 and 17. Plus signs in Figures 20 and 21 are the ice thickness values for positive uncertainties in the indicated variables; minus signs show the direction of change in ice thickness for a decrease in the controlling variable value.

Table 16. Sensitivity of ice thickness estimates to uncertainties in the controlling variables during daytime case with reference ice thickness of 1 meter.

Name	*Ref. Value*	*Error (Dx)*		*IceThk_Dh*		*IceThk_Dh/h*		*IceThk_Dh/Dx*	
T_s *(K)*	253.23	+2.000	-2.000	-0.235	+0.245	-0.235	+0.245	-0.117	-0.122
T_i *(K)*	253.23	+5.000	-5.000	-0.008	+0.008	-0.008	+0.008	-0.002	-0.002
h_s *(m)*	0.20	+0.100	-0.100	-0.654	+0.654	-0.654	+0.654	-6.544	-6.544
R (%)	90.00	+9.000	-9.000	+0.024	-0.024	+0.024	-0.024	+0.003	+0.003
U (m/s)	5.00	+1.000	-1.000	+0.316	-0.208	+0.316	-0.208	+0.316	+0.208
P_a *(hPa)*	1000.00	+50.00	-50.00	+0.066	-0.063	+0.066	-0.063	+0.001	+0.001
α_s *(0~1)*	0.85	+0.100	-0.100	-0.757	+2.195	-0.757	+2.195	-7.566	-21.953
T_r *(0~1)*	0.05	+0.050	-0.050	-0.086	+0.092	-0.086	+0.092	-1.711	-1.848
F_r *(w/m^2)*	101.44	+20.288	-20.288	+0.395	-0.295	+0.395	-0.295	+0.019	+0.015
F_a *(w/m^2)*	0.00	+2.000	-2.000	-0.212	+0.260	-0.212	+0.260	-0.106	+0.130
C (0~1)	0.50	+0.250	-0.250	+0.297	-0.639	+0.297	-0.639	+1.189	+2.555

Table 17. Sensitivity of ice thickness estimates to uncertainties in the controlling variables during nighttime case with reference ice thickness of 1 meter.

Name	***Ref. Value***	***Error (Dx)***		***IceThk_Dh***		***IceThk_Dh/h***		***IceThk_Dh/Dx***	
T_s (K)	241.09	+2.000	-2.000	-0.172	+0.179	-0.172	+0.179	-0.086	-0.090
T_i (K)	241.09	+5.000	-5.000	-0.008	+0.008	-0.008	+0.008	-0.002	-0.002
h_s (m)	0.20	+0.100	-0.100	-0.667	+0.667	-0.667	+0.667	-6.666	-6.666
R (%)	90.00	+9.000	-9.000	+0.006	-0.006	+0.006	-0.006	+0.001	+0.001
U (m/s)	5.00	+1.000	-1.000	+0.166	-0.133	+0.166	-0.133	+0.166	+0.133
P_a (hPa)	1000.00	+50.00	-50.00	+0.043	-0.041	+0.043	-0.041	+0.001	+0.001
F_a (w/m^2)	0.00	+2.000	-2.000	-0.137	+0.155	-0.137	+0.155	-0.068	0.078
C (0~1)	0.50	+0.250	-0.250	+0.248	-0.476	+0.248	-0.476	+0.992	+1.903

5 PRATICAL CONSIDERATIONS

5.1 Numerical Computation Considerations

This algorithm is implemented sequentially. Because ice thickness retrieval via OTIM relies on the values of the ancillary data flags, the ancillary data flags need to be computed first. This algorithm will be implemented into the AIT and uses its numerical routines for processing.

5.2 Programming and Procedural Considerations

This algorithm requires knowledge of spatial information for accurate pixel geographic locations and land mask information for identifying sea, lake, river, and et al. In addition, the temporal information is required for each pixel regarding the solar radiation in case daytime case is used. Beyond this reliance, this algorithm is purely a pixel by pixel algorithm.

5.3 Quality Assessment and Diagnostics

The following procedures are recommended for diagnosing the performance of this algorithm.

- Monitor the percentage of pixels retrieved for ice thickness, and check the value uniformity over the small and smooth area without cracks, melting ponds, and leads.
- Check input ancillary data such as surface skin temperature, air temperature, humidity, wind speed, and snow depth for all pixels of this algorithm. See how those ancillary variables changes affect ice thickness estimation.
- Periodically image the individual test results to look for artifacts or non-physical behaviors.
- Maintain a close collaboration with the other teams using this algorithm in their product generation.

5.4 Exception Handling

This algorithm includes checking the validity of input data before applying the OTIM and ice age algorithm. This algorithm also expects the main processing system (i.e. AIT) to flag any pixels with missing geolocation or viewing geometry information.

This algorithm does check for conditions where this algorithm cannot be performed. These conditions include missing input variables values and unsolvable numerical solutions. In these cases, the appropriate flag is set to indicate that no ice thickness and age are produced for that pixel.

5.5 Algorithm Validation

As discussed and detailed in section 4.2, the validations were performed with modeled ice thickness data from PIOMAS, submarine and mooring site measurements, and in-situ station measurements. Our testing and validations span the multiple years for every season, and cover both sea ice and lake ice, though most of them are within Arctic Ocean where the submarine, mooring sites, and station measurements were made for years.

The mean absolute error is 0.31 m for samples with a mean ice thickness of 1.80 m, i.e., a 17% mean absolute bias when comparing to the submarine uplooking sonar ice draft measurements in terms of ice thickness. The results of comparisons with mooring sites and in-situ Canadian station measurements are similar. In terms of ice age classifications, the algorithm can easily meet the MRD requirements by classifying ice into ice-free, first-year, and older ice with accuracy greater than 80% and product precision less than one category.

6 ASSUMPTIONS AND LIMITATIONS

The following sections describe the current limitations and assumptions in the current version of this algorithm.

6.1 Performance

The following list contains the current assumptions and proposed mitigation strategies.

1. Atmospheric profile and wind speed data are available from NWP or other teams' retrieved products. In case no profile data available, it is valid assumption as used by other researchers that surface air temperature generally is about 0.5 ~ 2 degree higher than ice/snow surface temperature depending on the cloud condition, and relative humidity is about 90% over ice/snow, and wind speed of 6~20 m/s at night. But wind speed should be observed or simulated to guarantee to be realistic.

2. Radiation fluxes are available from NWP or other teams' products; otherwise parameterizations will be used and assumed reliable and accurate enough for each pixel. (*Use parameterization schemes over ice and/or snow surface from Bennett (1982), Ohmura (1981), Jacob (1978) as recommended*).

3. Snow maps and climatological depths are available from NWP or other teams' products, or general assumption of 2~50 cm snow depth will be used over ice. (*Use snow information from NWP or elsewhere*).

4. Land mask maps are also available to identify different surface types.

5. All of the static ancillary data is available at the pixel level. (*Reduce the spatial resolution of the surface type, land mask and/or coast mask to pixel size*).

6.2 Assumed Sensor Performance

We assume the sensors will meet its current specifications and retrieved products from other teams will be accurate enough for this algorithm, otherwise this algorithm built-in parameterization schemes will be used for certain input variables. This algorithm will be critically dependent on the following retrieved products.

- Surface skin and air temperature.
- Radiation fluxes at the surface.
- Snow depth.
- Atmospheric moisture and wind.

6.3 Pre-Planned Product Improvements

This algorithm serves other applications. Its development is closely tied to the development and feedback from the other team algorithms. At this point, it is therefore difficult to predict what the future modifications will be. However, the following discussion contains our current best guess of the future modifications.

6.3.1 Daytime Algorithm Modification

The solar radiation is inevitably involved in the daytime ice thickness retrieval, making the OTIM extremely difficult to solve analytically for ice thickness due to the complicated ice/snow micro-macro physical properties in solar spectrum, which vary a lot with changes of ice/snow clarity, density, chemicals contained, salinity, particle size and shape, structure, and thickness itself that are hard to know beforehand. In this version, we have developed a regression method to estimate residual heat flux for both day and night times which now includes the contribution from solar radiation and surface ice/snow albedo for daytime cases. Therefore the new improved algorithm in this version can now be solved for daytime ice thickness analytically by using the previous nighttime algorithm. With the new uniform algorithm for both day and night ice thickness/age can be solved analytically along with the new regression method to estimate day and night residual heat flux.

6.3.2 Optimization

The OTIM has been optimized to minimize computation time. Other ways to optimize product generation will continue to be investigated.

7 REFERENCES

Andreas, E.L. and S.F. Ackley, 1982, On the differences in ablation seasons of Arctic and Antarctic sea ice, *J. Atmos. Sci.*, 39, 440-447.

Bennett, T.J., 1982, A coupled atmosphere-sea ice model study of the role of sea ice in climatic predictability, *J. Atmos. Sci.*, 39, 1456-1465.

ABDERRAHIM BENTAMY, KRISTINA B. KATSAROS, ALBERTO M. MESTAS-NUN˜ EZ, WILLIAM M. DRENNAN, EVAN B. FORDE,1 AND HERVE´ ROQUET, 2003, Satellite Estimates of Wind Speed and Latent Heat Flux over the Global Oceans, *J. Climate*, Vol.16, 637-656, 2003.

Berliand, T. C., 1960: Method of climatological estimation of global radiation. *Meteor. Gidrol.*, 6, 9-12.

Burt, W.V., 1954, Albedo over wind roughened water, *Journal of Meteorology*, 11, 283-290.

Chernigovskiy, N.T., 1963, Radiation properties of the central Arctic ice cover, Trudy Arkticheskogo I Antarkticheskogo Nauchno-Issledovatel'skogo Instituta, Tom 253, 249-260.

Cox, G.F.N. and W.F. Weeks, 1974, Salinity variations in sea ice, *J. Glaciol.*, 13, 109-120.

Curry, A. Judith and Peter J. Webster, 1999, <<Thermodynamics of Atmospheres & Oceans>>, pp.277, ISBN 0-12-199570-4, Academic Press.

Doronin, Y.P., 1971, Thermal Interaction of the Atmosphere and Hydrosphere in the Arctic, P.85, *Israel Program for Sci. Trans.*, Jerusalem, 1971.

Ebert, E. and J.A. Curry, 1993: An intermediate one-dimensional thermodynamic sea ice model for investigating ice-atmosphere interactions. *J. Geophys. Res.*, 98, 10085-10109.

Efimove, N.A., 1961, On methods of calculating monthly values of net longwave radiation, *Meteorol. Gidrol.*, 10, 28-33.

Fowler, C., J. Maslanik, T. Haran, T. Scambos, J. Key, and W. Emery. 2002. AVHRR Polar Pathfinder twice-daily 25 km EASE-Grid composites. Boulder, CO: National Snow and Ice Data Center. *Digital media*.

Grenfell, T. C. and G. A. Maykut, 1977, The optical properties of ice and snow in the Arctic Basin, *J. Glaciol.*, 18, 445-63.

Grenfell, T. C., 1979, The effects of ice thickness on the exchange of solar radiation over the polar oceans, *J. Glaciol.*, 22, 305-20.

Grenfell, T.C. and D.K. Perovich, 1984, Spectral albedos of sea ice and incident solar irradiance in the southern Beaufort Sea, *Journal of Geophysical Research*, Vol.89, C7, p. 3573-3580.

Grenfell, T.C. and D.K. Perovich, 2004, Seasonal and spatial evolution of albedo in a snow-ice-land-ocean environment, *J. Geophy. Res.*, 109, No. C1.

Jacobs, J.D., 1978: Radiation climate of Broughton Island. In: R. G. Barry and J. D. Jacobs, Energy budget studies in relation to fast-ice breakup processes in Davis Strait, Occas. Pap. 26,105-120. Inst. of Arctic and Alp. Res., Univ. of Colorado, Boulder, CO.

Jin, Z., K. Stamnes, and W.F. Weeks, 1994, The effect of sea ice on the solar energy budget in the atmosphere-sea ice-ocean system: A model Study, *J. Geophys. Res.*, 99, No. C12, 25,281-25,294.

Kara, A.B., P.A. Rochford, and H.E. Hurlburt, 2000, Efficient and Accurate Bulk Parameterizations of Air–Sea Fluxes for Use in General Circulation Models, *J. of Atmosph. and Oceanic Tech.*, Vol.17, 1421-1438, 2003.

Kemp, J., K. Newhall, W. Ostrom, R. Krishfield, and A. Proshutinsky (2005), The Beaufort Gyre Observing System 2004: Mooring Recovery and Deployment Operations in Pack Ice, Technical Report of the Woods Hole Oceanographic Institution, WHOI-2005-05, 33pp.

Key, 2002, The Cloud and Surface Parameter Retrieval (CASPR) System for Polar AVHRR, NOAA/NESDIS/STAR, Madison, WI, available online at the http://stratus.ssec.wisc.edu.

Key, J.R., R.A. Silcox, and R.S. Stone, 1996, Evaluation of surface radiative flux parameterizations for use in sea ice models, *J. Geophys. Res.*, Vol.101, No. C2, 3839-3849.

Key, J.R., A.J. Schweiger, and R.S. Stone, 1997, Expected uncertainty in satellite-derived estimates of the surface radiation budget at high latitudes, *J. Geophys. Res.*, Vol.102, No. C7, 15,837-15,847.

Kovacs, A., 1996. Sea ice: Part I. Bulk salinity versus ice floe thickness. US Army Cold Regions Research and Engineering Laboratory, CRREL Report 96-7.

Laevastu, T., 1960, Factors affecting the temperature of the surface layer of the sea, *Comments Phys. Math.*, 25, 1.

Langleben, M.P., 1971, Albedo of melting sea ice in the southern Beaufort Sea, *Journal of Glaciology*, 10, 101-104.

Lindsay, R.W., 1998, Temporal Variability of the Energy Balance of Thick Arctic Pack Ice, *J. Climate*, Vol.11, 313-333, March 1998.

Maslanik, J. A., J. R. Key, C. W. Fowler, T. Nguyen, and X.Wang, 2001: Spatial and temporal variability of satellite-derived cloud and surface characteristics during FIRE-ACE. *J. Geophys. Res.*, 106 (D14), 15 233–15 249.

Maslanik, J.A., C. Fowler, J. Stroeve, S. Drobot, J. Zwally, D. Yi, and W. Emery, 2007, A younger, thinner Arctic ice cover: Increased potential for rapid, extensive sea-ice loss, *Geophys. Res. Lett.*, 34, L24501, doi:10.1029/2007GL032043.

Maykut, G.A., and N. Untersteuner, 1971, Some results from a time-dependent thermodynamic model of sea ice, *J.G.R.*, Vol. 76, pp.1550-1575.

Maykut, G.A. and P.E. Church, 1973, Radiation climate of Barrow, Alaska, 1962-66, *J. Appl. Meteorol.*, 12, 620-628.

Moritz, R.E., 1978. A model for estimating global solar radiation, Energy budget studies in relation to fast-ice breakup processes in Davis Strait, edited by R.G. Barry and J.D. Jacobs, Occas.l Pap. 26pp. 121-142, Inst. Of Arctic and Alp. Res., Univ. of Colo., Boulder.

National Snow and Ice Data Center. 1998, updated 2006. Submarine upward looking sonar ice draft profile data and statistics. Boulder, CO: National Snow and Ice Data Center/World Data Center for Glaciology. *Digital media*.

Ohmura, A., 1981, Climate and energy balance of the Arctic tundra, Zürcher Geogr. Schr. 3, 448 pp., Geogr. Inst., Zürich, Switzerland.

Ostrom, W., J. Kemp, R. Krishfield, and A. Proshutinsky (2004), Beaufort Gyre Freshwater Experiment: Deployment Operations and Technology in 2003, Technical Report of the Woods Hole Oceanographic Institution, WHOI-2004-01, 32 pp.

Perovich, D.K., 1996, The Optical Properties of Sea Ice, *CRREL Monograph, 96-1.* 25 pp., May.

Rees, W.G., 1993, Infrared emissivities of Arctic land cover types, *Int. J. Remote Sensing*, 14, 1013-1017.

Schmetz, P.J. and E. Raschke, 1986, Estimation of daytime downward longwave radiation at the surface from satellite and grid point data, *Theor. Appl. Climatol.*, 37, 136-149.

Schmit, Timothy J., Mathew M. Gunshor, W. Paul Menzel, James J. Gurka, Jun Li, A. Scott Bachmeier, 2005: Introducing the next-generation Advanced Baseline Imager on GOES-R. Bull. Amer. Meteor. Soc., 86, 1079-1096

Schrodere, D., T. Vihma, A. Kerber and B. Brummer, 2003, On the parameterization of turbulent surface fluxes over heterogeneous sea ice surfaces, *J. Geophys. Res.*, 108 (C6), doi:10.1029/2002JC001385.

Shine, K.P., 1984, Parameterization of shortwave flux over high albedo surfaces as a function of cloud thickness and surface albedo, *Q. J. R. Meteorol. Soc.*, 110, 747-764.

Shine, K.P. and A. Henderson-Sellers, 1985, The sensitivity of a thermodynamic sea ice model to changes in surface albedo parameterization, *J. Geophys. Res.*, 90, 2243-2250.

Taylor, J.R., An Introduction to Error Analysis, 270 pp., Univ. Sci. Books, Mill Valley, Calif., 1982.

Thorndike, A. S., D. A. Rothrock, G. A. Maykut, and R. Colony, 1975: The thickness distribution of sea ice, *J. Geophys. Res.*, 80, 4501-4513.

Tucker, W.B., III, J.W.Weatherly, D.T. Eppler, L.D. Farmer, and D.L. Bentley, 2001, Evidence for rapid thinning of sea ice in the western Arctic Ocean at the end of the 1980s, *Geophys. Res. Lett.*, 28(14), 2851-2854.

Tuomo M. Saloranta, 2000, Modeling the evolution of snow, snow ice and ice in the Baltic Sea, *Tellus*, 52A, 93-108.

Thornedike, A.S., D.A. Rothrock, G.A. Maykut, and R.Colony, 1975, The thickness distribution of sea ice, *J. Geophys. Res.*, 80, 4501-4513.

Untersteiner, N., 1964, Calculations of temperature regime and heat budget of sea ice in the central Arctic, *J. Geophys. Res.*, 69, 4655-4766.

Wang, X. and J. Key, 2003, Recent trends in Arctic surface, cloud, and radiation properties from space, *Science*, 299(5613), 1725-1728.

Wang, X., J. Key, and Y. Liu, 2010, A thermodynamic model for estimating sea and lake ice thickness with optical satellite data, *J. Geophys. Res.*, revision submitted, Sept. 2010.

Yen, Y.-C., 1981: Review of thermal properties of snow, ice and sea ice. CRREL Rep. 81-10, 27 pp. [*Available from Cold Regions Research and Engineering Laboratory, 72 Lyme Rd., Hanover, NH 03755.*]

Yu, Y. and D.A. Rothrock, 1996, Thin ice thickness from satellite thermal imagery, *J. Geophys. Res.*, Vol.101, No. C10, 25,753-25,766.

Yu, Y., G.A. Maykut, and D.A. Rothrock, 2004, Changes in the thickness distribution of Arctic sea ice between 1958-1970 and 1993-1997, *J. Geophys. Res.*, 109, C08004, doi:10.1029/2003JC001982.

Zhang, J., and D.A. Rothrock, 2003, Modeling global sea ice with a thickness and enthalpy distribution model in generalized curvilinear coordinates, *Mon. Wea. Rev.*, 131(5), 681-697.

Zhang, J., and D.A. Rothrock, 2001, A thickness and enthalpy distribution sea-ice model, *J. Phys. Oceanogr.*, 31, 2986-33001.

Zillman, J.W., 1972, A study of some aspects of the radiation and heat budgets of the southern hemisphere oceans, Meteorol. Stud. Rep. 26, Bur. Of Meteorol., Dep. Of the Inter., Canberra, A.C.T.

Appendix A. Conductive heat flux for two-layer system with snow over ice

Consider a two-layer system, with a slab of ice overlaid by a layer of snow as shown below. We assume the temperature gradients in the snow and ice are each linear and thus conductive heat

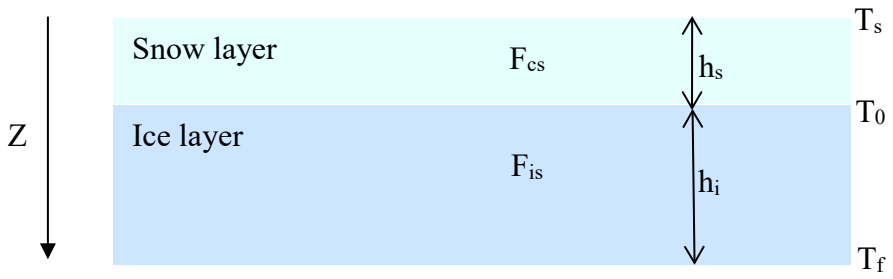

flux is constant with depth. At the snow/ice interface, the conductive flux in the snow must equal the conductive flux in the ice, i.e., $F_{ci} = F_{cs}$. As we define the direction to the snow/ice is positive, so we can derive the conductive heat flux for the two-layer system with a snow layer overlaid a slab of ice as shown below. Downward direction is defined positive, so F_c=k·dT/dh, where dT is temperature difference, and dh is the snow/ice thickness.

$F_c = k\frac{dT}{dZ}$, and so for the snow layer, we have $F_{cs} = k_s\frac{T_0 - T_s}{h_s}$, and the same for the ice slab,

$F_{ci} = k_s\frac{T_f - T_0}{h_i}$, so we have $k_s\frac{T_f - T_0}{h_i} = k_s\frac{T_0 - T_s}{h_s}$, after series of derivation, we finally get

$T_0 = \frac{k_s h_i T_s + k_i h_s T_f}{k_i h_s + k_s h_i}$, therefore $F_{cs} = \frac{k_i k_s}{k_i h_s + k_s h_i}(T_f - T_s)$, $F_c = F_{cs} = \frac{k_i k_s}{k_i h_s + k_s h_i}(T_f - T_s)$.